A generalised algorithm for anelastic processes in elastoplasticity and biomechanics

A Generalised Algorithm for Anelastic Processes in Elastoplasticity and Biomechanics*

Alfio Grillo†, Raphael Prohl‡, Gabriel Wittum§

DOI: https://doi.org/10.1177/1081286515598661. Available online: September 15, 2015
Journal: *Mathematics and Mechanics of Solids* (SAGE)

Abstract

A computational algorithm for solving anelastic problems in finite deformations is introduced. The presented procedure, termed Generalised Plasticity Algorithm (GPA) hereafter, takes inspiration from the Return Mapping Algorithm (RMA), which is typically employed to solve the Karush-Kuhn-Tucker (KKT) system arising in finite Elastoplasticity, but aims to modify and extend the RMA to the case of more general flow rules and strain energy density functions as well as to non-classical formulations of Elastoplasticity, in which the plastic variables are not treated as internal variables. To assess its reliability, the GPA is tested in two different contexts. Firstly, it is used for solving two classical problems (a shear-compression test and the necking of a circular bar). In both cases, the GPA is compared to the RMA in terms of structural set-up, computational effort and flexibility, and its convergence is evaluated by solving several benchmarks. Some restrictions of the classical form of the RMA are pointed out, and it is shown how these can be overcome by adopting the proposed algorithm. Secondly, the GPA is applied to characterise the mechanical response of a biological tissue that undergoes large deformations and remodelling of its internal structure.

Keywords: Finite Strain Elastoplasticity, Return Mapping Algorithm, Generalised Plasticity Algorithm.

1 Introduction

Anelastic processes constitute a widely investigated research subject of both theoretical and computational Mechanics. They play an important role in the characterisation of the mechanical response of continuum bodies that undergo reorganisations of their internal structure, besides deforming under the action of applied stimuli.

The interest in the evolution of the internal structure of continuum bodies ranges over various physical contexts, including industrial and biomechanical problems. In the case of industrial applications, a confident description of the elastoplastic behaviour of building materials, such as metals, is necessary to characterise their mechanical properties under

*Dedicated to Prof. R. A. Toupin, in recognition of his contributions to science.

†Corresponding Author. DISMA "G. L. Lagrange", Politecnico di Torino. Corso Duca degli Abruzzi 24, I-10129, Torino (TO), Italy. Tel.: +39 011 090 7531. Fax: +39 011 090 7599. E-mail: alfio.grillo@polito.it

‡Steinbeis Center, Simulation in Technology, Bussardweg 6, D-75446 Wiernsheim, Germany. E-mail: raphael@techsim.org

§G-CSC, Goethe Universität Frankfurt. Kettenhofweg 139, D-60325, Frankfurt am Main, Germany. E-mail: wittum@gcsc.uni-frankfurt.de

severe working conditions. In Biomechanics, the mathematical description of anelastic processes is required, for instance, to study the growth and remodelling (structural adaptation) of biological tissues. These phenomena are of great importance in the evolution and differentiation of tissues both in physiological and pathological situations, and apply to bone, articular cartilage, blood vessels and tumours. In all these cases, efficient and robust numerical methods have to be supplied to simulate reliably the material response.

Although the physics behind the onset of anelastic distortions in industrial materials is very different from that inherent in biological tissues, the mathematical models and the computational strategies addressing anelastic problems share many common features, and take inspiration from the Theory of Elastoplasticity, a rich research theme to which many authors have contributed (cf., e.g., [1, 2] and the references therein), and in which many efforts have been put for developing numerical methods (cf., e.g., [3, 4, 5, 6, 7, 8, 9]). In addition, reference should be made to the fundamental theories of Toupin [10] and Mindlin [11, 12].

To the best of the authors' knowledge and understanding, the crucial differences among the various models of Elastoplasticity arise when the issues of plastic flow and hardening are addressed. Taking for granted the Bilby-Kröner-Lee (BKL) multiplicative decomposition of the deformation gradient into an elastic and a plastic part, and describing hardening through a suitable hardening variable (in general, a second-order tensor field), the classical models of Elastoplasticity often treat the tensor of plastic distortions and the hardening variable as internal variables (cf., e.g., [13, 14, 15]). This is, however, not always the case. Indeed, both in Elastoplasticity and in the Biomechanics of tissue remodelling, there exist theories in which the tensor of plastic distortions is viewed as a kinematic entity that, together with the standard motion, determines the kinematics of a body [16, 17]. Another aspect, in which models of Plasticity differ from each other, is the formulation of the flow rule. Many models assume associative flow rules, which means that the plastic strain rate is derivable from the function defining the yield surface of the considered material [1]. In other circumstances, instead, non-associative flow rules must be considered (cf., e.g., [18]).

In Biomechanics, the BKL decomposition was introduced by Rodriguez *et al.* [19], who associated the processes of growth and remodelling with the occurrence of anelastic distortions. In [20], the anelastic distortions accompanying growth were interpreted as "local rearrangement of material inhomogeneities", and their evolution was shown to be driven by the Mandel stress tensor. In the theories of tumour growth [21] and remodelling of cellular aggregates [22], the "evolving natural configurations" [23] were exploited to define the anelastic distortions related with these processes.

A common computational method used to solve elastoplastic problems is the Return Mapping Algorithm (RMA). In its classical form, the RMA is a closest point projection method, presented under the hypotheses of associative flow rule and isotropic elastoplastic material behaviour [15]. The elastoplastic problem is reduced to a constrained optimisation problem, subjected to a set of Karush-Kuhn-Tucker (KKT-) conditions. Other algorithms have their origin in optimisation theory, like, e.g., the methods of Sequential Quadratic Programming (SQP) [24].

This manuscript sets itself two scopes. The first one is to present an algorithm that, on the one hand, can be applied to complex, non-linear anelastic problems (such as those involving the derivatives of plastic distortions) and that, on the other hand, may serve as a basis for developing an efficient solver for Structural Mechanics. Since it has been conceived as a generalisation of the classical RMA, and it has been applied for solving both elastoplastic problems of industrial interest and biomechanical problems of tissue remodelling, the proposed procedure has been named Generalised Plasticity Algorithm

(GPA). The GPA accounts for geometric and kinematic non-linearities, as well as for the non-linear constitutive behaviour of the considered materials.

The GPA is formulated in two contexts. In the first one, it aims to be an alternative to the classical RMA for elastoplastic models that fail to comply with all the hypotheses on which the standard RMA is based. To encompass more general flow rules, and to account for the cases in which the flow rules cannot be decoupled from the weak form of the momentum balance law, the GPA requires a linearisation with respect to the deformation and one with respect to the tensor of anelastic distortions. This means that, compared with the classical RMA, an additional linearisation iteration is performed in the GPA. In contrast to the SQP method, the GPA is not found by formulating a sequence of quadratic subproblems. Rather, the KKT-system is linearised with respect to the deformation and the tensor of anelastic distortions in the full non-linear elastoplastic regime.

The second scope of this work is to highlight the connection between mathematical modelling and numerics. Indeed, the GPA, which is inspired by the theories developed in [16, 17], stems from the fact that a model in which the standard motion and the anelastic distortions are viewed as equally ranked kinematic descriptors (rather than as a kinematic descriptor and an internal tensor variable) naturally requires a reformulation of the Principle of Virtual Powers. This, in turn, leads to the necessity of adapting the already well-established numerical methods of inelastic processes to more general solution strategies, thereby including novel discretisation schemes and linearisation algorithms.

Although the computational effort required by the GPA is higher than that of the RMA, the GPA seems to be more versatile and applicable to a wider variety of flow rules, elastoplastic behaviours, formulations of Elastoplasticity, and biomechanical problems.

The paper is organised as follows. Section 2 summarises the theoretical basis of the work. In section 3, all constitutive assumptions are reviewed in detail. In section 4, the two types of problems addressed in the paper, referred to as 'Pr1' and 'Pr2', are formalised. Section 5 is dedicated to review the RMA, while the proposed algorithm, the GPA, is presented in section 6. The problem 'Pr1' encompasses the von Mises J_2 theory of isochoric and associative plasticity, and is solved by applying both the standard RMA and the GPA in order to evaluate the functionality of the latter algorithm. The problem 'Pr2' is formulated in a more general framework, and its applicability to the biomechanical context is evidenced. The numerical results are shown in section 7, where the differences between the GPA and the RMA are discussed in detail. The philosophy of the work and some ideas for future research are discussed in section 8.

2 Theoretical Background

The formalism adopted hereafter follows [25], with some modifications. In the following, $\mathcal{B}$ is the three-dimensional manifold describing a solid body, $\mathcal{S}$ is the three-dimensional Euclidean space and $\mathcal{I} \subseteq \mathbb{R}$ is the interval of time over which the evolution of the body is observed. A motion is the one-parameter family of smooth mappings $\chi(\,\cdot\,, t) : \mathcal{B} \to \mathcal{S}$, with $t \in \mathcal{I}$. The set $\mathcal{C}_t = \chi(\mathcal{B}, t) \subset \mathcal{S}$ is referred to as current configuration. For every $X \in \mathcal{B}$ and $t \in \mathcal{I}$, there exists a spatial point $x \in \mathcal{C}_t$ such that $x = \chi(X, t)$. In the following, $\mathcal{S}$ is assumed to be equipped with the structure of affine space.

Given the space of free vectors $\mathcal{V}$, obtained by translating the points of $\mathcal{S}$, the space $T_x\mathcal{S} = \{\boldsymbol{v}_x \in \mathcal{V} \mid \boldsymbol{v}_x = y - x, y \in \mathcal{S}\}$ is the tangent space of $\mathcal{S}$ at x. Its dual space $T_x^*\mathcal{S}$ is the cotangent space at x. The disjoint unions $T\mathcal{S} = \sqcup_{x\in\mathcal{S}} T_x\mathcal{S}$ and $T^*\mathcal{S} = \sqcup_{x\in\mathcal{S}} T_x^*\mathcal{S}$ are the tangent bundle and cotangent bundle, respectively. With analogous notation, $T_X\mathcal{B}$ denotes the tangent space of $\mathcal{B}$ at X, and its dual space, $T_X^*\mathcal{B}$, is the cotangent space at X. Then,

$T\mathcal{B} = \sqcup_{X\in\mathcal{B}} T_X\mathcal{B}$ and $T^*\mathcal{B} = \sqcup_{X\in\mathcal{B}} T^*_X\mathcal{B}$ are the tangent bundle and the cotangent bundle of $\mathcal{B}$, respectively.

The velocity of a material particle passing through $x = \chi(X,t)$ at time t is denoted by $\boldsymbol{v}(x,t) \in T_x\mathcal{S}$. It holds that $\boldsymbol{v}(x,t) = \boldsymbol{u}(X,t) = \dot{\chi}(X,t)$, where the superimposed dot stands for partial differentiation with respect to time, and $\boldsymbol{u}(\,\cdot\,,t) : \mathcal{B} \to T\mathcal{S}$ is defined by $\boldsymbol{u}(X,t) = \boldsymbol{v}(\chi(X,t),t)$. The tangent map of $\chi(\,\cdot\,,t)$ at X, with $t \in \mathcal{I}$, is the deformation gradient tensor $T\chi(X,t) = \boldsymbol{F}(X,t) : T_X\mathcal{B} \to T_{\chi(X,t)}\mathcal{S}$, with $J := \det(\boldsymbol{F}) > 0$ for all $t \in \mathcal{I}$ and for all $X \in \mathcal{B}$.

Given the metric tensor $\boldsymbol{g} : T\mathcal{S} \to T^*\mathcal{S}$, the pull-back of $\boldsymbol{g}$ through χ is the right Cauchy-Green deformation tensor $\boldsymbol{C} = \boldsymbol{F}^{\mathrm{T}}.\boldsymbol{F} = \boldsymbol{F}^{\mathrm{T}}\boldsymbol{g}\boldsymbol{F} : T\mathcal{B} \to T^*\mathcal{B}$, with $\boldsymbol{F}^{\mathrm{T}} : T^*\mathcal{S} \to T^*\mathcal{B}$. The tensor $\boldsymbol{G} : T\mathcal{B} \to T^*\mathcal{B}$ is the material metric tensor.

The second-order tensor field $\boldsymbol{\ell}(\,\cdot\,,t) : \mathcal{B} \to T\mathcal{S} \otimes T^*\mathcal{S}$ is the velocity gradient expressed in terms of the points of $\mathcal{B}$, i.e. $\boldsymbol{\ell}(X,t) = \operatorname{grad}\boldsymbol{v}(x,t)$, with $x = \chi(X,t)$. It is related to the material velocity gradient, $\operatorname{Grad}\boldsymbol{u} = \dot{\boldsymbol{F}}$, through $\boldsymbol{\ell} = \dot{\boldsymbol{F}}\boldsymbol{F}^{-1}$. It holds that $\dot{\boldsymbol{C}} = \boldsymbol{F}^{\mathrm{T}} 2\boldsymbol{d}\boldsymbol{F}$, where $\boldsymbol{d} = \operatorname{sym}(\boldsymbol{\ell}^\flat)$ denotes the symmetric part of $\boldsymbol{\ell}^\flat = \boldsymbol{g}\boldsymbol{\ell} : T\mathcal{S} \to T^*\mathcal{S}$.

Sometimes the kinematics of a continuum body is formulated in terms of one chosen reference configuration rather than in terms of $\mathcal{B}$. Some words of caution on possible abuses of the concept of 'reference configuration' are given in [17, 20, 26].

2.1 Bilby-Kröner-Lee Decomposition of the Deformation Gradient

One of the theoretical pillars of finite Elastoplasticity is the multiplicative decomposition of $\boldsymbol{F}$ into an elastic and a plastic part [27]:

$$\boldsymbol{F} = \boldsymbol{F}_{\mathrm{e}}\boldsymbol{F}_{\mathrm{p}}. \tag{1}$$

In (1), $\boldsymbol{F}$ accounts for the global change of shape of the body, $\boldsymbol{F}_{\mathrm{p}}$ describes the total plastic distortions responsible for the evolution of the body's internal structure, and $\boldsymbol{F}_{\mathrm{e}}$ represents the total elastic distortion (in Kröner's terminology [27], a 'distortion' is the superposition of deformation and rotation). A thorough explanation of the physics behind (1) can be found, e.g., in [2]. The tensor field $\boldsymbol{F}_{\mathrm{p}}(\,\cdot\,,t)$ transforms the body elements of $\mathcal{B}$ into a collection $\mathcal{K}_t$ of stress-free body elements, which is referred as 'body's natural state'. The whole elastic distortion, $\boldsymbol{F}_{\mathrm{e}}$, is the distortion that has to be applied to the elements of $\mathcal{K}_t$ to get the global configuration $\mathcal{C}_t$. Since the body elements collected in the conglomerate $\mathcal{K}_t$ may become geometrically incompatible, $\mathcal{K}_t$ does not generally form a configuration in the Euclidean space. However, a continuous stress-free configuration can be reconstructed in some suitably defined non-Euclidean space [2, 27], whose curvature is induced by incompatibility. The body's natural state is not unique, since it is defined up to an orthogonal transformation [17, 28].

If (1) is viewed as the composition of tangent bundle maps [29], it is possible to introduce the mapping $\chi_\kappa(\,\cdot\,,t) : \mathcal{B} \to \mathcal{S}$ that serves as the base map for the bundle map $\boldsymbol{F}_{\mathrm{p}}$. The set $\mathcal{C}_\kappa = \chi_\kappa(\mathcal{B},t) \subset \mathcal{S}$, which represents the subregion of space $\mathcal{S}$ associated with the body's natural state, is termed 'intermediate configuration'. The total plastic distortion can be identified with the map $\boldsymbol{F}_{\mathrm{p}}(X,t) : T_X\mathcal{B} \to T_{\chi_\kappa(X,t)}\mathcal{S}$, even though $\boldsymbol{F}_{\mathrm{p}}$ is not the tangent map to χ_κ. Accordingly, the total elastic distortion is written as $\boldsymbol{F}_{\mathrm{e}}(X,t) \equiv \boldsymbol{F}(X,t)\boldsymbol{F}_{\mathrm{p}}^{-1}(X,t) : T_{\chi_\kappa(X,t)}\mathcal{S} \to T_{\chi(X,t)}\mathcal{S}$. To complete the physical frame within which $\boldsymbol{F}_{\mathrm{p}}$ and $\boldsymbol{F}_{\mathrm{e}}$ are conceived, the concepts of material uniformity and homogeneity should be discussed [26, 30, 31].

Granted the multiplicative decomposition (1), and denoting by $\boldsymbol{\eta}(\xi)$ the metric tensor associated with $T_\xi\mathcal{S}$, where $\xi = \chi_\kappa(X,t)$, one can define $\boldsymbol{b}_{\mathrm{e}} = \boldsymbol{F}_{\mathrm{e}}.\boldsymbol{F}_{\mathrm{e}}^{\mathrm{T}} = \boldsymbol{F}_{\mathrm{e}}\boldsymbol{\eta}^{-1}\boldsymbol{F}_{\mathrm{e}}^{\mathrm{T}}$ and

$\boldsymbol{B}_\mathrm{p} = \boldsymbol{F}_\mathrm{p}^{-1}\boldsymbol{\eta}^{-1}\boldsymbol{F}_\mathrm{p}^{-\mathrm{T}}$. The former is the left Cauchy-Green tensor generated by the elastic distortions, while the latter is the inverse of $\boldsymbol{C}_\mathrm{p} = \boldsymbol{F}_\mathrm{p}^{\mathrm{T}}.\boldsymbol{F}_\mathrm{p} = \boldsymbol{F}_\mathrm{p}^{\mathrm{T}}\boldsymbol{\eta}\boldsymbol{F}_\mathrm{p}$, i.e. the right Cauchy-Green tensor induced by the plastic distortions. It holds that $\boldsymbol{b}_\mathrm{e} = \boldsymbol{F}\boldsymbol{B}_\mathrm{p}\boldsymbol{F}^{\mathrm{T}}$.

The decomposition (1) also implies that the velocity gradient $\boldsymbol{\ell}$ splits additively as

$$\boldsymbol{\ell} = \boldsymbol{\ell}_\mathrm{e} + \underbrace{\boldsymbol{F}_\mathrm{e}\boldsymbol{L}_\mathrm{p}\boldsymbol{F}_\mathrm{e}^{-1}}_{:=\boldsymbol{\ell}_\mathrm{p}} = \boldsymbol{\ell}_\mathrm{e} + \boldsymbol{\ell}_\mathrm{p}, \tag{2}$$

where $\boldsymbol{\ell}_\mathrm{e} = \dot{\boldsymbol{F}}_\mathrm{e}\boldsymbol{F}_\mathrm{e}^{-1}$ and $\boldsymbol{L}_\mathrm{p} = \dot{\boldsymbol{F}}_\mathrm{p}\boldsymbol{F}_\mathrm{p}^{-1}$ denote, respectively, the rates of elastic and plastic distortions. The rates of $\boldsymbol{b}_\mathrm{e}$ and $\boldsymbol{B}_\mathrm{p}$ are related to each other by means of the expressions

$$\mathcal{L}_{\boldsymbol{v}}\boldsymbol{b}_\mathrm{e} = \boldsymbol{F}\dot{\overline{[\boldsymbol{F}^{-1}\boldsymbol{b}_\mathrm{e}\boldsymbol{F}^{-\mathrm{T}}]}}\boldsymbol{F}^{\mathrm{T}} = \boldsymbol{F}\dot{\boldsymbol{B}}_\mathrm{p}\boldsymbol{F}^{\mathrm{T}}, \tag{3a}$$

$$\dot{\boldsymbol{B}}_\mathrm{p} = -\boldsymbol{F}^{-1}\boldsymbol{F}_\mathrm{e}(\boldsymbol{\eta}^{-1}2\boldsymbol{D}_\mathrm{p}\boldsymbol{\eta}^{-1})\boldsymbol{F}_\mathrm{e}^{\mathrm{T}}\boldsymbol{F}^{-\mathrm{T}}, \tag{3b}$$

where $\mathcal{L}_{\boldsymbol{v}}\boldsymbol{b}_\mathrm{e}$ is the Lie derivative of $\boldsymbol{b}_\mathrm{e}$, while $\boldsymbol{D}_\mathrm{p} = \mathrm{sym}(\boldsymbol{\eta}\boldsymbol{L}_\mathrm{p})$ is the symmetric part of the fully covariant tensor $\boldsymbol{\eta}\boldsymbol{L}_\mathrm{p}$.

Another consequence of (1) is the decomposition $J = J_\mathrm{e}J_\mathrm{p}$, where $J_\mathrm{e} := \det(\boldsymbol{F}_\mathrm{e}) > 0$ and $J_\mathrm{p} := \det(\boldsymbol{F}_\mathrm{p}) > 0$ are the volumetric parts of the elastic and plastic distortions, respectively. The time derivatives of J_e and J_p are related to the traces of $\boldsymbol{\ell}_\mathrm{e}$ and $\boldsymbol{\ell}_\mathrm{p}$ by the expressions $\dot{J}_\mathrm{e} = J_\mathrm{e}\mathrm{tr}(\boldsymbol{\ell}_\mathrm{e})$ and $\dot{J}_\mathrm{p} = J_\mathrm{p}\mathrm{tr}(\boldsymbol{L}_\mathrm{p}) = J_\mathrm{p}\mathrm{tr}(\boldsymbol{\ell}_\mathrm{p})$. Furthermore, by defining the deformation gradient tensor as $\boldsymbol{F} = J^{1/3}\overline{\boldsymbol{F}}$ [32, 33], an expression is obtained in which $J^{1/3}\boldsymbol{i}$ and $\overline{\boldsymbol{F}}$ represent, respectively, the purely volumetric contribution and the volume-preserving part of the overall deformation (here, $\boldsymbol{i} : T\mathcal{S} \to T\mathcal{S}$ is the identity tensor in $T\mathcal{S}$). Thus, from (1) and the identity $J = J_\mathrm{e}J_\mathrm{p}$, it follows that $\overline{\boldsymbol{F}} = \overline{\boldsymbol{F}}_\mathrm{e}\overline{\boldsymbol{F}}_\mathrm{p}$.

A usual assumption both in metal plasticity and in the biomechanics of remodelling of biological tissues is that plastic distortions are isochoric, i.e. they must comply with the constraint $J_\mathrm{p} = 1$. This requirement places the restriction

$$\dot{J}_\mathrm{p} = -\tfrac{1}{2}[\det(\boldsymbol{B}_\mathrm{p})]^{-1/2}\,\mathrm{tr}(\boldsymbol{B}_\mathrm{p}^{-1}\dot{\boldsymbol{B}}_\mathrm{p}) = 0, \tag{4}$$

which means that the time derivative of $\boldsymbol{B}_\mathrm{p}$ is orthogonal to $\boldsymbol{B}_\mathrm{p}^{-1}$ in the sense that their double contraction vanishes identically, i.e. $\mathrm{tr}(\boldsymbol{B}_\mathrm{p}^{-1}\dot{\boldsymbol{B}}_\mathrm{p}) \equiv \boldsymbol{B}_\mathrm{p}^{-1} : \dot{\boldsymbol{B}}_\mathrm{p} = 0$. When (4) applies, the relation (3b) becomes

$$\dot{\overline{\boldsymbol{B}}}_\mathrm{p} = -\boldsymbol{F}^{-1}\boldsymbol{F}_\mathrm{e}(\boldsymbol{\eta}^{-1}2\,\mathrm{dev}(\boldsymbol{D}_\mathrm{p})\boldsymbol{\eta}^{-1})\boldsymbol{F}_\mathrm{e}^{\mathrm{T}}\boldsymbol{F}^{-\mathrm{T}}, \tag{5}$$

where $\mathrm{dev}(\boldsymbol{D}_\mathrm{p}) = \boldsymbol{D}_\mathrm{p} - \frac{1}{3}\mathrm{tr}\left(\boldsymbol{\eta}^{-1}\boldsymbol{D}_\mathrm{p}\right)\boldsymbol{\eta}$ is the deviatoric part of $\boldsymbol{D}_\mathrm{p}$, and $\overline{\boldsymbol{B}}_\mathrm{p} = \overline{\boldsymbol{F}}_\mathrm{p}^{-1}.\overline{\boldsymbol{F}}_\mathrm{p}^{-\mathrm{T}}$ is the volume-preserving part of $\boldsymbol{B}_\mathrm{p}$. Since the condition $J_\mathrm{p} = 1$ is enforced, (5) remains invariant under the substitution of $\boldsymbol{F}$ and $\boldsymbol{F}_\mathrm{e}$ with $\overline{\boldsymbol{F}}$ and $\overline{\boldsymbol{F}}_\mathrm{e}$, respectively.

Decompositions of the type (1) were proposed by many authors in problems related to growth and remodelling of biological tissues, which were studied either as monophasic continua [20, 21, 34, 35, 36, 37] or as mixtures [38, 39, 40, 41, 42, 43, 44]. A review on constitutive theories relying on (1) was done in [45].

2.2 Principle of Virtual Powers and Dissipation

Only a purely mechanical framework is considered hereafter. The body mass is assumed to be conserved. Thus, if ϱ denotes the spatial mass density of the body, and ϱ_R is its backward Piola transform (i.e. $\varrho_\mathrm{R}(X,t) = J(X,t)\varrho(\chi(X,t),t)$), the mass balance law reduces to $\dot{\varrho}_\mathrm{R} = 0$, which holds at all $X \in \mathcal{B}$ and for all $t \in \mathcal{I}$, i.e. $\varrho_\mathrm{R}(X,t) \equiv \varrho_\mathrm{R}(X)$ for all times.

Within the classical theory of finite Elastoplasticity, the elastoplastic behaviour of a body is described by its motion, χ, the plastic part of the total deformation, $\boldsymbol{F}_{\mathrm{p}}$, and the hardening variable $\boldsymbol{\alpha}$. In the standard theory, these three types of variables are not treated in same way, at least conceptually. Indeed, while χ is the solution of the set of equations governing the body dynamics, $\boldsymbol{F}_{\mathrm{p}}$ and $\boldsymbol{\alpha}$ are regarded as internal variables determined by solving evolution laws [13, 15, 46], which are not introduced on the same footing as χ. In other words, neither $\boldsymbol{F}_{\mathrm{p}}$ nor $\boldsymbol{\alpha}$ appear explicitly in the formulation of the Principle of Virtual Powers (PVP), which is established by defining the set of virtual (test) velocities as the collection of all admissible realisations of the type

$$\tilde{\mathcal{H}} := \{\tilde{\boldsymbol{u}} : \mathcal{B} \to T\mathcal{S} \mid \ \tilde{\boldsymbol{u}}_{|\partial\mathcal{B}_{\mathrm{D}}} = \boldsymbol{0}\}. \tag{6}$$

In (6), $\partial\mathcal{B}_{\mathrm{D}}$ is the Dirichlet-boundary of $\mathcal{B}$, i.e. the portion of $\partial\mathcal{B}$ over which position boundary conditions are enforced, and $\tilde{\boldsymbol{u}}_{|\partial\mathcal{B}_{\mathrm{D}}}$ is the restriction of $\tilde{\boldsymbol{u}}$ to $\partial\mathcal{B}_{\mathrm{D}}$.

For a first-grade material, the PVP reads

$$\int_{\mathcal{B}} \boldsymbol{P} : \boldsymbol{g}\mathrm{Grad}\,\tilde{\boldsymbol{u}} = \int_{\mathcal{B}} \boldsymbol{b}_{\mathrm{R}}.\tilde{\boldsymbol{u}} \ + \ \int_{\partial\mathcal{B}_{\mathrm{N}}} \boldsymbol{f}_{\mathrm{R}}.\tilde{\boldsymbol{u}}\,, \qquad \forall\ \tilde{\boldsymbol{u}} \in \tilde{\mathcal{H}}\,, \tag{7}$$

and expresses the weak form of the local balance of momentum. In (7), $\boldsymbol{P}{:}T^*\mathcal{B} \to T\mathcal{S}$ is the first Piola-Kirchhoff stress tensor (it is related to Cauchy stress by the Piola transformation $\boldsymbol{\sigma}(\chi(X,t),t) = [J(X,t)]^{-1}\boldsymbol{P}(X,t)\boldsymbol{F}^{\mathrm{T}}(X,t)^{1}$); $\boldsymbol{b}_{\mathrm{R}}(X,t) = J(X,t)\boldsymbol{b}(\chi(X,t),t)$ is the body force per unit volume of $\mathcal{B}$ (whereas $\boldsymbol{b}$ is the body force per unit volume of $\mathcal{C}_t$), and collects both inertial force and long-range interactions; $\boldsymbol{f}_{\mathrm{R}}$ expresses the contact forces $\boldsymbol{f}$, which act on the boundary of the current configuration, per unit area of $\partial\mathcal{B}$; finally, $\partial\mathcal{B}_{\mathrm{N}}$ is the Neumann-boundary of $\mathcal{B}$, i.e. the portion of $\partial\mathcal{B}$ over which surface forces are applied (it holds that $\partial\mathcal{B}_{\mathrm{D}} \cup \partial\mathcal{B}_{\mathrm{N}} = \partial\mathcal{B}$, and $\partial\mathcal{B}_{\mathrm{D}} \cap \partial\mathcal{B}_{\mathrm{N}} = \emptyset$). The forces $\boldsymbol{f}_{\mathrm{R}}$ and $\boldsymbol{f}$ are reciprocally related by [47]

$$\boldsymbol{f}_{\mathrm{R}}(X,t) = J(X,t)\boldsymbol{f}(\chi(X,t),t)\sqrt{\boldsymbol{N}(X).\boldsymbol{C}^{-1}(X,t).\boldsymbol{N}(X)}, \quad (X,t) \in \partial\mathcal{B}_{\mathrm{N}} \times \mathcal{I}. \tag{8}$$

The left- and the right-hand-side of (7), denoted by $\mathcal{P}_{\mathrm{int}}(\tilde{\boldsymbol{u}})$ and $\mathcal{P}_{\mathrm{ext}}(\tilde{\boldsymbol{u}})$, are defined over $\tilde{\mathcal{H}}$, and are referred to as virtual internal power and virtual external power, respectively.

A standard localisation argument associates (7) with its corresponding strong form

$$\mathrm{Div}(\boldsymbol{P}) = -\boldsymbol{b}_{\mathrm{R}}, \qquad \text{in } \mathcal{B} \times \mathcal{I}, \tag{9a}$$

$$\boldsymbol{P}.\boldsymbol{N} = \boldsymbol{f}_{\mathrm{R}}, \qquad \text{on } \partial\mathcal{B}_{\mathrm{N}} \times \mathcal{I}, \tag{9b}$$

$$\boldsymbol{P}\boldsymbol{F}^{\mathrm{T}} = \boldsymbol{F}\boldsymbol{P}^{\mathrm{T}}, \qquad \text{in } \mathcal{B} \times \mathcal{I}. \tag{9c}$$

In (9b), $\boldsymbol{N}$ is the unit vector normal to $\partial\mathcal{B}_{\mathrm{N}}$. Equation (9c) follows from the physical condition that $\mathcal{P}_{\mathrm{int}}(\tilde{\boldsymbol{u}})$ must satisfy the Principle of Material Frame Indifference.

The dissipation associated with a fixed region $\Omega \in \mathcal{B}$ is defined by [16]

$$\int_{\Omega} D_{\mathrm{R}} = -\overline{\int_{\Omega} \psi_{\mathrm{R}}}^{\cdot} \ + \ \mathcal{P}_{\mathrm{net}}(\Omega) \geq 0\,, \tag{10}$$

where D_{R} is the dissipation density, ψ_{R} is the body's stored energy function, and the net power $\mathcal{P}_{\mathrm{net}}(\Omega)$ is defined as

$$\mathcal{P}_{\mathrm{net}}(\Omega) = \int_{\partial\Omega} (\boldsymbol{P}.\boldsymbol{N}).\boldsymbol{u} \ + \int_{\Omega} \boldsymbol{b}_{\mathrm{R}}.\boldsymbol{u} = \int_{\Omega} \boldsymbol{P}{:}\boldsymbol{g}\mathrm{Grad}\,\boldsymbol{u}\,. \tag{11}$$

[1]Rigorously speaking, $\boldsymbol{F}^{\mathrm{T}}$ should be expressed as a functions of x and t. That is, in introducing the Piola transformation of $\boldsymbol{\sigma}$, we are committing the slight abuse of notation $\boldsymbol{F}^{\mathrm{T}}(X,t) \equiv \boldsymbol{F}^{\mathrm{T}}(\chi(X,t),t)$.

By substituting (11) into (10), and localising the results, one obtains

$$D_{\mathrm{R}} = -\dot{\psi}_{\mathrm{R}} + \boldsymbol{S} : \tfrac{1}{2}\dot{\boldsymbol{C}} \geq 0\,, \tag{12}$$

where $\boldsymbol{S} = \boldsymbol{F}^{-1}\boldsymbol{P} : T^{*}\mathcal{B} \to T\mathcal{B}$ is the second Piola-Kirchhoff stress tensor. By introducing the quantities $\psi_{\kappa} = J_{\mathrm{p}}^{-1}\psi_{\mathrm{R}}$ and $D_{\kappa} = J_{\mathrm{p}}^{-1}D_{\mathrm{R}}$, (12) transforms as follows

$$D_{\kappa} = -\dot{\psi}_{\kappa} + \boldsymbol{S}_{\kappa} : \boldsymbol{F}_{\mathrm{p}}^{-\mathrm{T}}\tfrac{1}{2}\dot{\boldsymbol{C}}\boldsymbol{F}_{\mathrm{p}}^{-1} \geq 0\,, \tag{13}$$

with $\boldsymbol{S}_{\kappa} = J_{\mathrm{p}}^{-1}\boldsymbol{F}_{\mathrm{p}}\boldsymbol{S}\boldsymbol{F}_{\mathrm{p}}^{\mathrm{T}}$ being the second Piola-Kirchhoff stress tensor associated with $\mathcal{C}_{\kappa}$.

3 Constitutive Theory

If the material under study is uniform, the constitutive description of its inelastic behaviour can be done by having recourse to the Principle of Material Uniformity [13, 20, 26, 30, 48, 49, 50], and the stored energy ψ_{κ} can be expressed constitutively as a function depending solely on the tensor of elastic distortions, $\boldsymbol{F}_{\mathrm{e}}$, and the hardening variable. Moreover, since constitutive laws must be objective, it must hold that $\hat{\psi}_{\mathrm{R}}(\boldsymbol{F}, \boldsymbol{F}_{\mathrm{p}}, \alpha, X) = J_{\mathrm{p}}\hat{\psi}_{\kappa}(\boldsymbol{C}_{\mathrm{e}}, \alpha)$, with $\boldsymbol{C}_{\mathrm{e}} = \boldsymbol{F}_{\mathrm{e}}^{\mathrm{T}}\boldsymbol{g}\boldsymbol{F}_{\mathrm{e}}$ being the Cauchy-Green tensor of elastic distortions. The hardening parameter α is introduced with respect to $\mathcal{C}_{\kappa}$, and is assumed to be a scalar in the following.

3.1 Decoupling of the Stored Energy Function

To simplify the forthcoming calculations, the stored energy function $\hat{\psi}_{\kappa}(\boldsymbol{C}_{\mathrm{e}}, \alpha)$ is given in the decoupled form [15]

$$\hat{\psi}_{\kappa}(\boldsymbol{C}_{\mathrm{e}}, \alpha) = \hat{W}_{\kappa}(\boldsymbol{C}_{\mathrm{e}}) + \hat{\mathfrak{H}}_{\kappa}(\alpha)\,, \tag{14}$$

where $\hat{\mathfrak{H}}_{\kappa}(\alpha)$ is referred to as hardening potential. By substituting the time derivative of $\hat{\psi}_{\kappa}$ into (13), and hypothesising that the material exhibits hyperelastic behaviour from $\mathcal{C}_{\kappa}$, the following results are obtained:

$$\boldsymbol{S}_{\kappa} = 2\frac{\partial\hat{\psi}_{\kappa}}{\partial\boldsymbol{C}_{\mathrm{e}}} = 2\frac{\partial\hat{W}_{\kappa}}{\partial\boldsymbol{C}_{\mathrm{e}}}\,, \tag{15a}$$

$$\boldsymbol{\Sigma} = \boldsymbol{\eta}^{-1}\boldsymbol{C}_{\mathrm{e}}\boldsymbol{S}_{\kappa}\,, \tag{15b}$$

$$q = -\frac{\partial\hat{\psi}_{\kappa}}{\partial\alpha} = -\frac{\partial\hat{\mathfrak{H}}_{\kappa}}{\partial\alpha}\,, \tag{15c}$$

$$D_{\kappa} = \boldsymbol{\Sigma} : \boldsymbol{\eta}\boldsymbol{L}_{\mathrm{p}} + q\dot{\alpha} \geq 0\,. \tag{15d}$$

Given $\hat{W}_{\kappa}$ and $\hat{\mathfrak{H}}_{\kappa}$ explicitly, $\boldsymbol{S}_{\kappa}$, the Mandel stress tensor $\boldsymbol{\Sigma}$, and the generalised force q dual to the hardening rate $\dot{\alpha}$ are expressed constitutively by (15a), (15b) and (15c), respectively. Since it has been assumed that anelastic (plastic) distortions are isochoric, $\boldsymbol{L}_{\mathrm{p}}$ is trace-free, which implies that only the deviatoric part of $\boldsymbol{\Sigma}$ is constrained by the residual dissipation inequality (15d). Moreover, a consequence of the decoupled form of the stored energy function is that the stress does not depend on the hardening function and, similarly, the force-like variable q does not depend on deformation.

3.2 Isotropy

Although there exist theoretical models and computational algorithms elaborated for finite-strain elastoplasticity of anisotropic materials (cf., e.g., [51, 52, 53, 54, 55]), the

majority of the numerical methods rely, to the authors' knowledge, on the hypothesis of isotropic material behaviour [2, 15, 24, 46, 56].

There are at least two big advantages implied by isotropy. The first one is that the issue of plastic spin does not arise at all (see, e.g., [30]); the second advantage is that the flow rule can be formulated in terms of $\boldsymbol{B}_\mathrm{p}$, so that no evolution law for $\boldsymbol{F}_\mathrm{p}$ is actually needed (in some cases —e.g., for polycrystals [57]— evolution laws for $\boldsymbol{F}_\mathrm{p}$ are prescribed, in accordance to Mandel's isoclinicity rule [2], under the assumption of vanishing plastic rotations, so that the plastic variable is either $\boldsymbol{V}_\mathrm{p}$ or $\boldsymbol{U}_\mathrm{p}$, depending on whether the right or the left decomposition of $\boldsymbol{F}_\mathrm{p} = \boldsymbol{R}_\mathrm{p}.\boldsymbol{U}_\mathrm{p} = \boldsymbol{V}_\mathrm{p}.\boldsymbol{R}_\mathrm{p}$ is chosen).

For a hyperelastic isotropic material, the stored energy function $\hat{W}_\kappa$ depends on $\boldsymbol{C}_\mathrm{e}$ exclusively through its invariants, i.e.

$$I_1 = \hat{I}_1(\boldsymbol{C}_\mathrm{e}) = \mathrm{tr}(\boldsymbol{\eta}^{-1}\boldsymbol{C}_\mathrm{e}) = \mathrm{tr}(\boldsymbol{B}_\mathrm{p}\boldsymbol{C})\,, \tag{16a}$$

$$I_2 = \hat{I}_2(\boldsymbol{C}_\mathrm{e}) = \tfrac{1}{2}\big\{[\hat{I}_1(\boldsymbol{C}_\mathrm{e})]^2 - \mathrm{tr}[(\boldsymbol{\eta}^{-1}\boldsymbol{C}_\mathrm{e})^2]\big\} = \tfrac{1}{2}\left\{I_1^2 - \mathrm{tr}(\boldsymbol{B}_\mathrm{p}\boldsymbol{C}\boldsymbol{B}_\mathrm{p}\boldsymbol{C})\right\}\,, \tag{16b}$$

$$I_3 = \hat{I}_3(\boldsymbol{C}_\mathrm{e}) = \det(\boldsymbol{C}_\mathrm{e}) = J^2\,. \tag{16c}$$

This property necessarily implies that the Mandel stress tensor $\boldsymbol{\Sigma}$, which by definition must satisfy the equality $\boldsymbol{\Sigma}\boldsymbol{C}_\mathrm{e}\boldsymbol{\eta}^{-1} = \boldsymbol{\eta}^{-1}\boldsymbol{C}_\mathrm{e}\boldsymbol{\Sigma}^\mathrm{T}$ (cf. (15b)), must be symmetric itself, i.e. $\boldsymbol{\Sigma} = \boldsymbol{\Sigma}^\mathrm{T}$. Indeed, by setting $\hat{W}_\kappa(\boldsymbol{C}_\mathrm{e}) = \hat{W}_\kappa(\hat{I}_1(\boldsymbol{C}_\mathrm{e}), \hat{I}_2(\boldsymbol{C}_\mathrm{e}), \hat{I}_3(\boldsymbol{C}_\mathrm{e}))$, one obtains

$$\boldsymbol{\Sigma} = 2\beta_1\boldsymbol{\eta}^{-1}\boldsymbol{C}_\mathrm{e}\boldsymbol{\eta}^{-1} + 2\beta_2[I_1\boldsymbol{\eta}^{-1}\boldsymbol{C}_\mathrm{e}\boldsymbol{\eta}^{-1} - \boldsymbol{\eta}^{-1}\boldsymbol{C}_\mathrm{e}\boldsymbol{\eta}^{-1}\boldsymbol{C}_\mathrm{e}\boldsymbol{\eta}^{-1}] + 2\beta_3 I_3\boldsymbol{\eta}^{-1}\,, \tag{17}$$

with $\{\beta_i = \frac{\partial\hat{W}_\kappa}{\partial I_i}\}_{i=1}^3$. Since $\boldsymbol{\Sigma}$ is symmetric, the first summand on the right-hand-side of (15d) becomes $\boldsymbol{\Sigma} : \boldsymbol{\eta}\boldsymbol{L}_\mathrm{p} = \boldsymbol{\Sigma} : \boldsymbol{D}_\mathrm{p}$, meaning that only the symmetric part of the rate of plastic distortions contributes to dissipation. This result rules out the plastic spin, i.e. the skew-symmetric part of $\boldsymbol{\eta}\boldsymbol{L}_\mathrm{p}$, which cannot thus be determined in terms of thermodynamic arguments [30]. Finally, by invoking the kinematic relations (3), the inequality (15d) can be rewritten as

$$D_\kappa = -\tfrac{1}{2}\left(\boldsymbol{g}\mathrm{dev}(\boldsymbol{\tau}_\kappa)\boldsymbol{b}_\mathrm{e}^{-1}\right) : \mathcal{L}_{\boldsymbol{v}}\boldsymbol{b}_\mathrm{e} + q\dot{\alpha} \geq 0\,, \tag{18}$$

where $\boldsymbol{\tau}_\kappa = \boldsymbol{F}_\mathrm{e}\boldsymbol{S}_\kappa\boldsymbol{F}_\mathrm{e}^\mathrm{T} = \boldsymbol{g}^{-1}\boldsymbol{F}_\mathrm{e}^{-\mathrm{T}}\boldsymbol{\eta}\boldsymbol{\Sigma}\boldsymbol{F}_\mathrm{e}^\mathrm{T}$ is the Kirchhoff stress tensor associated with the body's natural state. Furthermore, setting $\boldsymbol{\tau} = J_\mathrm{p}\boldsymbol{\tau}_\kappa$ (with $J_\mathrm{p} = 1$), it is also useful to introduce the material Mandel stress tensor $\boldsymbol{\Sigma}_\mathrm{R} = \boldsymbol{G}^{-1}\boldsymbol{F}^\mathrm{T}\boldsymbol{g}\boldsymbol{\tau}\boldsymbol{F}^{-\mathrm{T}}$. The constitutive expressions of $\boldsymbol{\tau}_\kappa$ and $\boldsymbol{\Sigma}_\mathrm{R}$ read

$$\hat{\boldsymbol{\tau}}_\kappa(\boldsymbol{F}, \boldsymbol{B}_\mathrm{p}) = 2\beta_1\boldsymbol{b}_\mathrm{e} + 2\beta_2\left(I_1\boldsymbol{b}_\mathrm{e} - \boldsymbol{b}_\mathrm{e}\boldsymbol{g}\boldsymbol{b}_\mathrm{e}\right) + 2\beta_3 I_3\boldsymbol{g}^{-1}\,, \tag{19a}$$

$$\hat{\boldsymbol{\Sigma}}_\mathrm{R}(\boldsymbol{F}, \boldsymbol{B}_\mathrm{p}) = (2\beta_1 + 2\beta_2 I_1)\boldsymbol{G}^{-1}\boldsymbol{C}\boldsymbol{B}_\mathrm{p} - 2\beta_2\boldsymbol{G}^{-1}\boldsymbol{C}\boldsymbol{B}_\mathrm{p}\boldsymbol{C}\boldsymbol{B}_\mathrm{p} + 2\beta_3 I_3\boldsymbol{G}^{-1}\,. \tag{19b}$$

The tensor $\boldsymbol{\Sigma}_\mathrm{R}$ is not symmetric in general, but it has the properties $\boldsymbol{\Sigma}_\mathrm{R}\boldsymbol{C}\boldsymbol{G}^{-1} = \left(\boldsymbol{\Sigma}_\mathrm{R}\boldsymbol{C}\boldsymbol{G}^{-1}\right)^\mathrm{T}$, $\boldsymbol{G}\boldsymbol{\Sigma}_\mathrm{R}\boldsymbol{B}_\mathrm{p}^{-1} = \left(\boldsymbol{G}\boldsymbol{\Sigma}_\mathrm{R}\boldsymbol{B}_\mathrm{p}^{-1}\right)^\mathrm{T}$ and $\boldsymbol{B}_\mathrm{p}\boldsymbol{G}\boldsymbol{\Sigma}_\mathrm{R} = \left(\boldsymbol{B}_\mathrm{p}\boldsymbol{G}\boldsymbol{\Sigma}_\mathrm{R}\right)^\mathrm{T}$. The first one follows from its own definition, while the second and the third one follow from isotropy [30].

3.3 Rate-Independent Plasticity and Yield Criterion

The hypothesis of rate-independent plasticity requires the introduction of a yield criterion [16]. To this end, let $\mathcal{T}_\tau$ and $\mathcal{T}_q$ be the spaces of Kirchhoff stresses and stress-like hardening functions q (cf. (15c)), and let $f_\tau : \mathcal{T}_\tau \times \mathcal{T}_q \to \mathbb{R}$ be a yield function defined by

$$f_\tau(\boldsymbol{\tau}_\kappa, q) = \varphi_\tau\left(\mathrm{dev}(\boldsymbol{\tau}_\kappa)\right) + \sqrt{\tfrac{2}{3}}\,[q - \tau_y], \tag{20}$$

where the positive parameter τ_y is the yield stress, and the function φ_τ depends on $\boldsymbol{\tau}_\kappa$ through the deviatoric part of it for consistency with (18).

The set $\mathcal{A} = \{(\boldsymbol{\tau}_\kappa, q) \in \mathcal{T}_\tau \times \mathcal{T}_q \,:\, f_\tau(\boldsymbol{\tau}_\kappa, q) \leq 0\}$ is referred to as the set of admissible stresses. In accordance with von Mises classical theory of J_2-plasticity, the function φ_τ is defined here as $\varphi_\tau\left(\mathrm{dev}(\boldsymbol{\tau}_\kappa)\right) = \|\mathrm{dev}(\boldsymbol{\tau}_\kappa)\| = \sqrt{\mathrm{tr}[(\boldsymbol{g}\mathrm{dev}(\boldsymbol{\tau}_\kappa))^2]}$. Consequently, one obtains

$$\frac{\partial f_\tau}{\partial \boldsymbol{\tau}_\kappa}(\boldsymbol{\tau}_\kappa, q) = \boldsymbol{g}\boldsymbol{n}\boldsymbol{g} \equiv \boldsymbol{n}^\flat, \quad \boldsymbol{n} = \frac{\mathrm{dev}(\boldsymbol{\tau}_\kappa)}{\|\mathrm{dev}(\boldsymbol{\tau}_\kappa)\|}, \tag{21}$$

with $\|\boldsymbol{n}\| = 1$. The inequality $f_\tau(\boldsymbol{\tau}_\kappa, q) < 0$ defines the instantaneous elastic range of the material. Plastic flow begins when the boundary of $\mathcal{A}$ is reached, i.e. when $f_\tau(\boldsymbol{\tau}_\kappa, q) = 0$.

3.4 Principle of Maximum Plastic Dissipation and Flow Rules

To formulate the Principle of Maximum Plastic Dissipation (PMPD), the dissipation $\mathcal{D}_\kappa$ (cf. (18)) has to be viewed as a non-negative, real-valued function defined over the set $\mathcal{A}$. The PMPD affirms that D_κ reaches its maximum when it is computed for the actual values of stress $\boldsymbol{\tau}_\kappa$ and hardening function q that characterise the material, i.e.

$$D_\kappa(\boldsymbol{\tau}_\kappa, q) = \max_{(\boldsymbol{r},\vartheta)\in\mathcal{A}} \{D_\kappa(\boldsymbol{r}, \vartheta)\}. \tag{22}$$

Since the maximisation is performed under the constraint that the pair $(\boldsymbol{r}, \vartheta) \in \mathcal{A}$ be admissible, the condition (22) allows to reformulate (18) into a constrained optimisation problem, which can be studied by introducing the Lagrangian function

$$L_\kappa(\boldsymbol{r}, \vartheta, \gamma_\tau) = D_\kappa(\boldsymbol{r}, \vartheta) - \gamma_\tau f_\tau(\boldsymbol{r}, \vartheta), \quad (\boldsymbol{r}, \vartheta) \in \mathcal{A}, \tag{23}$$

where γ_τ is an unknown Lagrange multiplier. Maximising (23) leads to the optimality conditions [15, 46]

$$\mathcal{L}_{\boldsymbol{v}}\boldsymbol{b}_\mathrm{e} = -2\gamma_\tau \boldsymbol{n}\boldsymbol{g}\boldsymbol{b}_\mathrm{e}\,, \tag{24a}$$

$$\dot{\alpha} = \gamma_\tau \sqrt{\frac{2}{3}}\,, \tag{24b}$$

$$\gamma_\tau \geq 0, \quad f_\tau(\boldsymbol{\tau}_\kappa, q) \leq 0, \quad \gamma_\tau f_\tau(\boldsymbol{\tau}_\kappa, q) = 0\,. \tag{24c}$$

Equations (24) determine the Karush-Kuhn-Tucker (KKT) system, and are also referred to as KKT-conditions. By invoking (3a), (24a) can be rewritten in terms of $\dot{\boldsymbol{B}}_\mathrm{p}$, i.e.

$$\dot{\boldsymbol{B}}_\mathrm{p} = -2\gamma_\tau \boldsymbol{F}^{-1}(\boldsymbol{n}\boldsymbol{g}\boldsymbol{b}_\mathrm{e})\boldsymbol{F}^{-\mathrm{T}}\,. \tag{25}$$

A consequence of (19a) is that the product $\boldsymbol{n}\boldsymbol{g}\boldsymbol{b}_\mathrm{e}$ is commutative. Moreover, by recalling the identity $\mathrm{dev}(\boldsymbol{\tau}) = \boldsymbol{g}^{-1}\boldsymbol{F}^{-\mathrm{T}}\boldsymbol{G}\,\mathrm{dev}(\boldsymbol{\Sigma}_\mathrm{R})\boldsymbol{F}^\mathrm{T}$, (25) becomes

$$\dot{\boldsymbol{B}}_\mathrm{p} = -2\gamma_\tau\, \boldsymbol{B}_\mathrm{p}\boldsymbol{G}\,\frac{\mathrm{dev}(\boldsymbol{\Sigma}_\mathrm{R})}{\|\mathrm{dev}(\boldsymbol{\tau})\|}\,. \tag{26}$$

According to (24c), γ_τ is zero when the material is in its elastic range, i.e. when $f_\tau(\boldsymbol{\tau}_\kappa, q) < 0$, and is greater than zero, when the yield surface is reached, i.e. when $f_\tau(\boldsymbol{\tau}_\kappa, q) = 0$. In the case in which γ_τ is positive, it is determined by the consistency condition $\gamma_\tau \dot{f}(\boldsymbol{\tau}_\kappa, q) = 0$, which leads to the expression

$$\gamma_\tau = \frac{\boldsymbol{n}^\flat : J_\mathrm{e}\mathbb{A} : \boldsymbol{d}}{\boldsymbol{n}^\flat : J_\mathrm{e}\mathbb{A} : \boldsymbol{n}^\flat + (2/3)\partial^2_\alpha \hat{\mathfrak{H}}_\kappa} = \frac{-\boldsymbol{n}^\flat : J_\mathrm{e}\mathbb{B}_\mathrm{p} : \frac{1}{2}\mathcal{L}_{\boldsymbol{v}}\boldsymbol{b}_\mathrm{e}}{\boldsymbol{n}^\flat : J_\mathrm{e}\mathbb{A} : \boldsymbol{n}^\flat}\,, \tag{27}$$

with

$$J_{\mathrm{e}}\mathbb{A} = J_{\mathrm{e}}\mathbb{C} + \boldsymbol{\tau}_\kappa \,\overline{\otimes}\, \boldsymbol{g}^{-1} + \boldsymbol{g}^{-1} \,\underline{\otimes}\, \boldsymbol{\tau}_\kappa \,, \tag{28a}$$

$$J_{\mathrm{e}}\mathbb{C} = \boldsymbol{F}_{\mathrm{e}} \,\underline{\otimes}\, \boldsymbol{F}_{\mathrm{e}} : \mathbb{C}_\kappa : \boldsymbol{F}_{\mathrm{e}}^{\mathrm{T}} \,\underline{\otimes}\, \boldsymbol{F}_{\mathrm{e}}^{\mathrm{T}}, \quad \mathbb{C}_\kappa = 4\frac{\partial^2 \hat{W}_\kappa}{\partial \boldsymbol{C}_{\mathrm{e}}^2}(\boldsymbol{C}_{\mathrm{e}}) \,, \tag{28b}$$

$$J\mathbb{B}_{\mathrm{p}} = \boldsymbol{F} \underline{\otimes} \boldsymbol{F} : \mathbb{B}_{\mathrm{p}} : \boldsymbol{F}^{-1} \underline{\otimes} \boldsymbol{F}^{-1} \,, \quad \mathbb{B}_{\mathrm{p}} = 2\frac{\partial \hat{\boldsymbol{S}}}{\partial \boldsymbol{B}_{\mathrm{p}}}(\boldsymbol{C}, \boldsymbol{B}_{\mathrm{p}}) \,. \tag{28c}$$

The fourth-order tensors $\mathbb{A}$ and $\mathbb{C}$ are referred to as tensor of the effective elastic moduli and spatial elasticity tensor, respectively. Moreover, $\boldsymbol{S} = \hat{\boldsymbol{S}}(\boldsymbol{C}, \boldsymbol{B}_{\mathrm{p}}) = J_{\mathrm{p}} \boldsymbol{F}_{\mathrm{p}}^{-1} \boldsymbol{S}_\kappa \boldsymbol{F}_{\mathrm{p}}^{-\mathrm{T}}$ is the constitutive expression of the material second Piola-Kirchhoff stress tensor. According to (27), the multiplier γ_τ (when it is nonzero) is defined as a function of $\boldsymbol{F}$, $\dot{\boldsymbol{F}}$, $\boldsymbol{B}_{\mathrm{p}}$ and α, i.e. $\gamma_\tau = \hat{\gamma}_\tau(\boldsymbol{F}, \dot{\boldsymbol{F}}, \boldsymbol{B}_{\mathrm{p}}, \alpha)$.

In conclusion, equations (24a) and (24b), largely adopted in von Mises J_2-theory of Elastoplasticity, can be reformulated as evolution laws for the plastic variables $\boldsymbol{B}_{\mathrm{p}}$ and α:

$$\dot{\boldsymbol{B}}_{\mathrm{p}} = \begin{cases} -\hat{\boldsymbol{\mathfrak{R}}}(\boldsymbol{F}, \dot{\boldsymbol{F}}, \boldsymbol{B}_{\mathrm{p}}, \alpha), & \text{if } \gamma_\tau = \hat{\gamma}_\tau(\boldsymbol{F}, \dot{\boldsymbol{F}}, \boldsymbol{B}_{\mathrm{p}}, \alpha) > 0 \quad (f_\tau(\boldsymbol{\tau}_\kappa, q) = 0) \,, \\ \boldsymbol{0} & \text{if } \gamma_\tau = 0 \,, \quad (f_\tau(\boldsymbol{\tau}_\kappa, q) < 0) \,, \end{cases} \tag{29a}$$

$$\dot{\alpha} = \begin{cases} \sqrt{\frac{2}{3}}\, \hat{\gamma}_\tau(\boldsymbol{F}, \dot{\boldsymbol{F}}, \boldsymbol{B}_{\mathrm{p}}, \alpha), & \text{if } \gamma_\tau = \hat{\gamma}_\tau(\boldsymbol{F}, \dot{\boldsymbol{F}}, \boldsymbol{B}_{\mathrm{p}}, \alpha) > 0 \quad (f_\tau(\boldsymbol{\tau}_\kappa, q) = 0) \,, \\ 0 & \text{if } \gamma_\tau = 0 \,, \quad (f_\tau(\boldsymbol{\tau}_\kappa, q) < 0) \,, \end{cases} \tag{29b}$$

where the negative of the tensor-valued function $\hat{\boldsymbol{\mathfrak{R}}}$ is defined by the right-hand-side of (26). Clearly, the definition of $\hat{\boldsymbol{\mathfrak{R}}}$ depends on the choice of the stored energy density function $\hat{W}_\kappa$, and of the hardening potential $\hat{\mathfrak{H}}_\kappa$.

3.5 Other Types of Flow Rules

In some biomechanical contexts, as those addressing the structural reorganisation of cell aggregates, plasticity-like models have been developed in which hardening is usually not accounted for, and the anelastic distortions model the reorganisation of the adhesion bonds connecting the cells. The onset of this type of anelastic processes is taken into account by introducing a yield stress in the constitutive laws. The symmetric part of the rate of plastic distortions is driven by stress according to laws of the type [58]

$$\boldsymbol{D}_{\mathrm{p}} = \zeta_{\mathrm{p}}\, \boldsymbol{\eta} \mathrm{dev}(\boldsymbol{\Sigma}) \boldsymbol{\eta} = \zeta_{\mathrm{p}}\, \boldsymbol{F}_{\mathrm{e}}^{\mathrm{T}} \boldsymbol{g} \mathrm{dev}(\boldsymbol{\tau}_\kappa)\, \boldsymbol{F}_{\mathrm{e}}^{-\mathrm{T}} \boldsymbol{\eta} \,, \tag{30}$$

where ζ_{p} is a plastic multiplier. By invoking (3b), the flow rule (30) becomes

$$\dot{\boldsymbol{B}}_{\mathrm{p}} = -2 \left(J_{\mathrm{p}}^{-1} \zeta_{\mathrm{p}} \right) \boldsymbol{B}_{\mathrm{p}} \boldsymbol{G} \mathrm{dev} \left(\boldsymbol{\Sigma}_{\mathrm{R}} \right) \,. \tag{31}$$

In (30) and (31), ζ_{p} is defined by[2]

$$\zeta_{\mathrm{p}} = J_{\mathrm{p}} \lambda \left[\frac{\varphi(\boldsymbol{\tau}) - \sqrt{(2/3)}\, \tau_y}{\varphi(\boldsymbol{\tau})} \right]_+ , \tag{32}$$

where λ is a non-negative phenomenological coefficient (with units $[\lambda] = (\mathrm{s} \cdot \mathrm{MPa})^{-1}$), $[\mathfrak{f}]_+ = \mathfrak{f}$, if $\mathfrak{f} > 0$, and $[\mathfrak{f}]_+ = 0$ otherwise, and $\varphi(\boldsymbol{\tau}) = \|\mathrm{dev}(\boldsymbol{\tau})\|$. Since the constraint

[2]The definition of γ_{p} given in [58] is slightly different from that reported here, where the expression of γ_{p} in (32) has been introduced for consistency with the rest of the paper.

$J_{\rm p} = 1$ applies, it holds that $\boldsymbol{\tau} = \boldsymbol{\tau}_\kappa$, and (31) becomes

$$\dot{\boldsymbol{B}}_{\rm p} = -2\gamma_{\rm p}\boldsymbol{B}_{\rm p}\boldsymbol{G}\frac{\mathrm{dev}(\boldsymbol{\Sigma}_{\rm R})}{\|\mathrm{dev}(\boldsymbol{\tau})\|}\,, \tag{33a}$$

$$\gamma_{\rm p} := \lambda\left[\|\mathrm{dev}(\boldsymbol{\tau})\| - \sqrt{(2/3)}\tau_y\right]_+\,, \tag{33b}$$

with $[\gamma_{\rm p}] = \mathrm{s}^{-1}$. Although $\gamma_{\rm p}$ is not a Lagrange multiplier, since it does not have to comply with a consistency condition of the type (27), the flow rule (33a) satisfies the dissipation inequality. Moreover, comparing (33a) with (26), one can show that the two flow rules are identical up to the specification of γ_τ and $\gamma_{\rm p}$. Thus, the right-hand-side of (33a) can be expressed by means of a tensor-valued function $\hat{\boldsymbol{\mathfrak{R}}}(\boldsymbol{F}, \boldsymbol{B}_{\rm p})$. The dependence on $\dot{\boldsymbol{F}}$ does not appear, since $\gamma_{\rm p}$ is not restricted by any KKT-consistency condition of the type (27).

4 Statement and Solution of the Problems 'Pr1' and 'Pr2'

For simplicity, the external forces $\boldsymbol{b}_{\rm R}$ and $\boldsymbol{f}_{\rm R}$ are set equal to zero from here on. Thus, it holds $\boldsymbol{P}.\boldsymbol{N} = \boldsymbol{0}$ on $\partial\mathcal{B}_{\rm N}$ (cf. (9b)). Consequently, the problem 'Pr1' can be stated as follows:

4.1 Problem 'Pr1'

Let $\hat{W}_\kappa(\boldsymbol{C}_{\rm e})$, $\hat{\mathfrak{H}}_\kappa(\alpha)$, f_τ, γ_τ, and $\boldsymbol{\mathfrak{R}}$ be given such that

$$\boldsymbol{P} = \hat{\boldsymbol{P}}(\boldsymbol{F}, \boldsymbol{B}_{\rm p}) = J_{\rm p}\hat{\boldsymbol{\tau}}_\kappa(\boldsymbol{F}, \boldsymbol{B}_{\rm p})\boldsymbol{F}^{-\mathrm{T}} = J_{\rm p}\left[\boldsymbol{F}_{\rm e}\left(2\frac{\partial\hat{W}_\kappa}{\partial\boldsymbol{C}_{\rm e}}(\boldsymbol{C}_{\rm e})\right)\boldsymbol{F}_{\rm e}^{\mathrm{T}}\right]\boldsymbol{F}^{-\mathrm{T}}\,, \tag{34a}$$

$$q = -K(\alpha) = -\frac{\partial\hat{\mathfrak{H}}_\kappa}{\partial\alpha}(\alpha)\,, \tag{34b}$$

$$\gamma_\tau = \begin{cases} 0, & \text{if } f_\tau(\boldsymbol{\tau}_\kappa, q) < 0, \\ \hat{\gamma}_\tau(\boldsymbol{F}, \dot{\boldsymbol{F}}, \boldsymbol{B}_{\rm p}, \alpha) > 0, & \text{if } f_\tau(\boldsymbol{\tau}_\kappa, q) = 0, \end{cases} \tag{34c}$$

$$\boldsymbol{\mathfrak{R}} = \begin{cases} \boldsymbol{0}, & \text{if } f_\tau(\boldsymbol{\tau}_\kappa, q) < 0, \\ \hat{\boldsymbol{\mathfrak{R}}}(\boldsymbol{F}, \dot{\boldsymbol{F}}, \boldsymbol{B}_{\rm p}, \alpha), & \text{if } f_\tau(\boldsymbol{\tau}_\kappa, q) = 0, \end{cases} \tag{34d}$$

where $\hat{\gamma}_\tau$ and $\hat{\boldsymbol{\mathfrak{R}}}$ are known functions of their arguments, with $\hat{\boldsymbol{\mathfrak{R}}}$ being specified in (25).

Find $\chi \in \mathcal{H}$, $\boldsymbol{B}_{\rm p} \in \mathbf{L}^2(\mathcal{B}\times\mathcal{I}, T\mathcal{B}\otimes T\mathcal{B})$ and $\alpha \in L^2(\mathcal{B}\times\mathcal{I}, \mathbb{R})$ such that

$$\mathcal{P}(\chi, \boldsymbol{B}_{\rm p}, \tilde{\boldsymbol{u}}) := \int_{\mathcal{B}} \hat{\boldsymbol{P}}(\boldsymbol{F}, \boldsymbol{B}_{\rm p}) : \boldsymbol{g}\mathrm{Grad}\,\tilde{\boldsymbol{u}} = 0, \qquad \forall\ \tilde{\boldsymbol{u}} \in \tilde{\mathcal{H}}, \tag{35a}$$

$$\dot{\boldsymbol{B}}_{\rm p} = -\boldsymbol{\mathfrak{R}}, \qquad \boldsymbol{B}_{\rm p}(X, 0) = \boldsymbol{B}_{\rm p0}(X) \text{ in } \mathcal{B}, \tag{35b}$$

$$\dot{\alpha} = \gamma_\tau\sqrt{\tfrac{2}{3}}, \qquad \alpha(X, 0) = \alpha_0(X) \text{ in } \mathcal{B}. \tag{35c}$$

Here, $\mathbf{L}^2(\mathcal{B}\times\mathcal{I}, T\mathcal{B}\otimes T\mathcal{B})$ and $L^2(\mathcal{B}\times\mathcal{I}, \mathbb{R})$ denote, respectively, the spaces of all tensor-valued and scalar-valued functions that are (Lebesgue) square-integrable in $\mathcal{B}$, while $\mathcal{H}$ is the subset of $\left(H^1(\mathcal{B}\times\mathcal{I}, \mathcal{S})\right)^3$ characterised by the property

$$\mathcal{H} = \left\{\chi \in \left(H^1(\mathcal{B}\times\mathcal{I}, \mathcal{S})\right)^3 :\ \ \chi(X, t) = \chi_{\rm b}(t),\ \forall\ (X, t) \in \partial\mathcal{B}_{\rm D}\times\mathcal{I}\right\}, \tag{36}$$

with $\left(H^1(\mathcal{B}\times\mathcal{I}, \mathcal{S})\right)^3$ being the Sobolev space of all functions $\chi(\,\cdot\,, t)$, $t \in \mathcal{I}$, valued in the three-dimensional Euclidean space $\mathcal{S}$ that are square-integrable in $\mathcal{B}$ and whose weak

derivatives $D^k\chi(\,\cdot\,,t)$, with $|k| \leq 1$, are all square-integrable in $\mathcal{B}$, too (here, k denotes a multi-index) [59]. Moreover, in (36), χ_{b} is the prescribed value of the motion on the body's Dirichlet-boundary $\partial\mathcal{B}_{\mathrm{D}}$. The space of virtual velocities $\tilde{\mathcal{H}}$ can now be identified with the functional space $\left(H_0^1(\mathcal{B},\mathcal{S})\right)^3$, i.e. $\tilde{\mathcal{H}} = \left(H_0^1(\mathcal{B},\mathcal{S})\right)^3$, which is the Hilbert subspace of $\left(H^1(\mathcal{B},\mathcal{S})\right)^3$ defined as the closure of the space of test-functions in $\left(H^1(\mathcal{B},\mathcal{S})\right)^3$, and characterised by the property that all functions $\tilde{\boldsymbol{u}} \in \left(H_0^1(\mathcal{B},\mathcal{S})\right)^3$ vanish on $\partial\mathcal{B}_{\mathrm{D}}$ [59].

The problem 'Pr1' (formulated by (34a)–(35c)) stems from the von Mises J_2 theory of isochoric and associative plasticity, since the rate of plastic distortions is deviatoric and proportional to the associated measure of stress. On the other hand, granted isotropy, and provided that $\boldsymbol{\mathcal{R}}$ complies with some restrictions related to dissipation (e.g., residual dissipation inequality [15], or maximisation of plastic work [2]), equation (35b) can also be generalised to comprehend many other types of flow rules, which might be even fully phenomenological, and need not be associative in general. For this reason, it is also useful to consider modified versions of 'Pr1', which do not strictly follow from the KKT-conditions (24), like, for instance, the problem referred to as 'Pr2' in this paper.

4.2 Problem 'Pr2'

Let $\hat{W}_\kappa(\boldsymbol{C}_{\mathrm{e}})$ and $\hat{\boldsymbol{\mathcal{R}}}(\boldsymbol{F},\boldsymbol{B}_{\mathrm{p}})$ be given, and let the first Piola-Kirchhoff stress tensor be defined by

$$\boldsymbol{P} = \hat{\boldsymbol{P}}(\boldsymbol{F},\boldsymbol{B}_{\mathrm{p}}) = J_{\mathrm{p}}\hat{\boldsymbol{\tau}}_\kappa(\boldsymbol{F},\boldsymbol{B}_{\mathrm{p}})\boldsymbol{F}^{-\mathrm{T}} = J_{\mathrm{p}}\left[\boldsymbol{F}_{\mathrm{e}}\left(2\frac{\partial\hat{W}_\kappa}{\partial\boldsymbol{C}_{\mathrm{e}}}(\boldsymbol{C}_{\mathrm{e}})\right)\boldsymbol{F}_{\mathrm{e}}^{\mathrm{T}}\right]\boldsymbol{F}^{-\mathrm{T}}. \tag{37}$$

Find $\chi \in \mathcal{H}$ and $\boldsymbol{B}_{\mathrm{p}} \in \mathbf{L}^2(\mathcal{B}\times\mathcal{I}, T\mathcal{B}\otimes T\mathcal{B})$ such that

$$\mathcal{P}(\chi,\boldsymbol{B}_{\mathrm{p}},\tilde{\boldsymbol{u}}) := \int_{\mathcal{B}} \hat{\boldsymbol{P}}(\boldsymbol{F},\boldsymbol{B}_{\mathrm{p}}) : \boldsymbol{g}\mathrm{Grad}\,\tilde{\boldsymbol{u}} = 0, \qquad \forall\ \tilde{\boldsymbol{u}} \in \tilde{\mathcal{H}}, \tag{38a}$$

$$\dot{\boldsymbol{B}}_{\mathrm{p}} = -\hat{\boldsymbol{\mathcal{R}}}(\boldsymbol{F},\boldsymbol{B}_{\mathrm{p}}), \qquad \boldsymbol{B}_{\mathrm{p}}(X,0) = \boldsymbol{B}_{\mathrm{p0}}(X) \text{ in } \mathcal{B}. \tag{38b}$$

The tensor-valued function $\hat{\boldsymbol{\mathcal{R}}}$ of the flow rule (38b) can be given, for example, by the right-hand-side of (33a), with γ_{p} defined in (33b) [58], or by more general expressions that lead to non-associative plasticity [2].

5 A Review of the Return Mapping Algorithm for 'Pr1'

Looking at some literature (see, e.g., [15, 46, 60]), the RMA is usually formulated under two hypotheses, which add themselves to those discussed in sections 3.1–3.4. The first hypothesis is that the strain energy density $\hat{W}_\kappa(\boldsymbol{C}_{\mathrm{e}})$ used in 'Pr1', can be decoupled into a pure volumetric contribution, $\hat{U}_\kappa(J_{\mathrm{e}})$, and a purely isochoric contribution, $\overline{W}_\kappa(\overline{\boldsymbol{C}}_{\mathrm{e}})$. In particular, a quasi-incompressible Neo-Hookean material is considered, i.e.

$$\hat{W}_\kappa(\boldsymbol{C}_{\mathrm{e}}) = \hat{U}_\kappa(J_{\mathrm{e}}) + \overline{W}_\kappa(\overline{\boldsymbol{C}}_{\mathrm{e}}), \tag{39a}$$

$$\hat{U}_\kappa(J_{\mathrm{e}}) = \tfrac{1}{2}\kappa\left\{\tfrac{1}{2}(J_{\mathrm{e}}^2-1) - \ln(J_{\mathrm{e}})\right\}, \tag{39b}$$

$$\overline{W}_\kappa(\overline{\boldsymbol{C}}_{\mathrm{e}}) = \tfrac{1}{2}\mu\left\{\mathrm{tr}\left(\boldsymbol{\eta}^{-1}\overline{\boldsymbol{C}}_{\mathrm{e}}\right) - 3\right\}, \tag{39c}$$

where κ and μ are the bulk and shear moduli, respectively, and $\boldsymbol{C}_{\mathrm{e}} = J_{\mathrm{e}}^{2/3}\overline{\boldsymbol{C}}_{\mathrm{e}}$ [32, 33], with $\det(\overline{\boldsymbol{C}}_{\mathrm{e}}) = 1$. In (39a)–(39c), as well as in all the following calculations, both $J_{\mathrm{e}} = \sqrt{\det(\boldsymbol{C}_{\mathrm{e}})}$ and $\overline{\boldsymbol{C}}_{\mathrm{e}}$ are to be regarded as functions of $\boldsymbol{C}_{\mathrm{e}}$. Direct consequences of this hypothesis are the equalities $\beta_1 = \frac{\mu}{2}J_{\mathrm{e}}^{-2/3}$ and $\beta_2 = 0$, which lead to $\mathrm{dev}(\boldsymbol{\tau}_\kappa) = \mu\,\mathrm{dev}(\overline{\boldsymbol{b}}_{\mathrm{e}})$, with $\overline{\boldsymbol{b}}_{\mathrm{e}} = J_{\mathrm{e}}^{-2/3}\boldsymbol{b}_{\mathrm{e}}$.

The second hypothesis is that the right-hand-side of (24a) can be approximated by $\frac{1}{3}\mathrm{tr}(\boldsymbol{g}\boldsymbol{b}_\mathrm{e})\boldsymbol{n}$, so that the flow rule becomes

$$\mathcal{L}_{\boldsymbol{v}}\boldsymbol{b}_\mathrm{e} = -\tfrac{2}{3}\gamma_\tau \mathrm{tr}(\boldsymbol{g}\boldsymbol{b}_\mathrm{e})\boldsymbol{n}. \tag{40}$$

This is obtained by enforcing the decomposition $\boldsymbol{b}_\mathrm{e} = \frac{1}{3}\mathrm{tr}(\boldsymbol{g}\boldsymbol{b}_\mathrm{e})\boldsymbol{g}^{-1} + \mathrm{dev}(\boldsymbol{b}_\mathrm{e})$ in (24a), and neglecting the term $\boldsymbol{n}\boldsymbol{g}\mathrm{dev}(\boldsymbol{b}_\mathrm{e})$ with respect to the right-hand-side of (40). To justify this approximation it suffices to notice that, when plastic flow occurs (i.e. when the condition $f_\tau(\boldsymbol{\tau}_\kappa, q) = 0$ is satisfied), $\boldsymbol{n}\boldsymbol{g}\mathrm{dev}(\boldsymbol{b}_\mathrm{e})$ becomes

$$\boldsymbol{n}\boldsymbol{g}\mathrm{dev}(\boldsymbol{b}_\mathrm{e}) = J_\mathrm{e}^{2/3}\frac{\|\mathrm{dev}(\boldsymbol{\tau}_\kappa)\|}{\mu}\boldsymbol{n}\boldsymbol{g}\boldsymbol{n} = J_\mathrm{e}^{2/3}\frac{\sqrt{\frac{2}{3}}\left(K(\alpha)+\tau_y\right)}{\mu}\boldsymbol{n}\boldsymbol{g}\boldsymbol{n}. \tag{41}$$

This result amounts to say that the term $\boldsymbol{n}\boldsymbol{g}\mathrm{dev}(\boldsymbol{b}_\mathrm{e})$ can be dropped because it is of the same order as the ratio between the yield stress in the presence of hardening, $\sqrt{\frac{2}{3}}(K(\alpha)+\tau_y)$, and the shear modulus, which is usually small for the majority of metals [46]. Even though, as stated by Simo [46], this approximation is not essential, it simplifies considerably the numerical treatment of the flow rule and the determination of γ_τ.

Although the strain energy density (39) reduces the computational effort (since it is independent of I_2), it might be unrealistic in some situations. In fact, it applies to elastically quasi-incompressible materials (for which J_e is close to unity), but fails to reproduce the correct elastic response of materials for which this assumption cannot be done. Indeed, the use of (39) for materials not satisfying quasi-incompressibility suppresses unjustifiably some independent elastic parameters from the material's elasticity tensor [61, 62, 63, 64, 65].

5.1 Algorithmic Determination of the KKT-Multiplier

This Section largely follows the theory reported in [15]. The crux of the RMA is describing the time-discrete evolution of $\boldsymbol{B}_\mathrm{p}$ and α jointly with the discretised KKT-conditions (24) and the weak form of the momentum balance (35a). For this purpose, at each instant of time $t_n \in \mathcal{I}$, $n \in \mathbb{N}$, the body is assumed to be characterised by two states: The *actual state* is that determined by the functions χ_n, $\boldsymbol{B}_{\mathrm{p}n}$ and α_n, which represent the actual solution of 'Pr1' at time t_n. The *trial state*, instead, is the one in which the body would find itself, if no plastic evolution took place within the time step $\Delta t_n = t_n - t_{n-1}$, $n \geq 1$. By definition, the trial state is determined by the functions χ_n^{trial}, $\boldsymbol{B}_{\mathrm{p}n}^{\mathrm{trial}} = \boldsymbol{B}_{\mathrm{p}(n-1)}$ and $\alpha_n^{\mathrm{trial}} = \alpha_{n-1}$, where χ_n^{trial} is the solution to (35a) at time t_n, if $\boldsymbol{B}_{\mathrm{p}n}$ were substituted in the constitutive expression of the first Piola-Kirchhoff stress tensor with the stepwise constant function $\boldsymbol{B}_{\mathrm{p}(n-1)}$ [15].

The introduction of the trial state, the particularly simple strain energy density specified in (39), and the approximated flow rule (40) allow to express the time-discrete form of (40) in terms of stress and, above all, to consider the stress at time t_n as a function of the deformation gradient and trial quantities only.

By recalling (3a), the Lie-derivative of $\boldsymbol{b}_\mathrm{e}$ at time $t_n \in \mathcal{I}$ is approximated by

$$\left(\mathcal{L}_{\boldsymbol{v}}\boldsymbol{b}_\mathrm{e}\right)_n = \boldsymbol{F}_n\frac{\boldsymbol{B}_{\mathrm{p}n} - \boldsymbol{B}_{\mathrm{p}(n-1)}}{\Delta t_n}\boldsymbol{F}_n^{\mathrm{T}}, \quad n \in \mathbb{N},\ n \geq 1, \tag{42}$$

where $\boldsymbol{F}_n$ is the tangent map of χ_n, and the time derivative $\dot{\boldsymbol{B}}_\mathrm{p}$ has been replaced by a finite difference. Moreover, substituting (42) into the left-hand-side of (40) leads to [15]

$$\overline{\boldsymbol{b}}_{\mathrm{e}n} = \overline{\boldsymbol{b}}_{\mathrm{e}n}^{\mathrm{trial}} - \tfrac{2}{3}\gamma_{\tau n}\Delta t_n \mathrm{tr}\big(\boldsymbol{g}\,\overline{\boldsymbol{b}}_{\mathrm{e}n}\big)\,\boldsymbol{n}_n, \tag{43}$$

with $\overline{\boldsymbol{b}}_{en} = J_{en}^{-2/3}\boldsymbol{b}_{en}$, $\boldsymbol{b}_{en} = \boldsymbol{F}_n\boldsymbol{B}_{pn}\boldsymbol{F}_n^{\mathrm{T}}$, $\overline{\boldsymbol{b}}_{en}^{\mathrm{trial}} = J_{en}^{-2/3}\boldsymbol{b}_{en}^{\mathrm{trial}}$, and $\boldsymbol{b}_{en}^{\mathrm{trial}} = \boldsymbol{F}_n\boldsymbol{B}_{\mathrm{p}(n-1)}\boldsymbol{F}_n^{\mathrm{T}}$, which implies that $\mathrm{tr}(\boldsymbol{g}\overline{\boldsymbol{b}}_{en}) = \mathrm{tr}(\boldsymbol{g}\overline{\boldsymbol{b}}_{en}^{\mathrm{trial}})$. Hence, taking the deviatoric part of both sides of (43), and multiplying the resulting expression by μ, one obtains

$$\boldsymbol{s}_n = \boldsymbol{s}_n^{\mathrm{trial}} - \tfrac{2}{3}\mu\gamma_{\tau n}\Delta t_n \mathrm{tr}\Big(\boldsymbol{g}\,\overline{\boldsymbol{b}}_{en}^{\mathrm{trial}}\Big)\,\boldsymbol{n}_n, \tag{44}$$

where the notation $\boldsymbol{s}_n = \mathrm{dev}(\boldsymbol{\tau}_{\kappa n}) = \mu\,\mathrm{dev}(\overline{\boldsymbol{b}}_{en})$, and $\boldsymbol{s}_n^{\mathrm{trial}} = \mu\,\mathrm{dev}(\overline{\boldsymbol{b}}_{en}^{\mathrm{trial}})$ has been used. Finally, setting $\boldsymbol{s}_n = \|\boldsymbol{s}_n\|\boldsymbol{n}_n$ and $\boldsymbol{s}_n^{\mathrm{trial}} = \|\boldsymbol{s}_n^{\mathrm{trial}}\|\boldsymbol{n}_n^{\mathrm{trial}}$, equation (44) can be rewritten as [15]

$$\Big[\|\boldsymbol{s}_n\| + \tfrac{2}{3}\mu\gamma_{\tau n}\Delta t_n \mathrm{tr}\Big(\boldsymbol{g}\,\overline{\boldsymbol{b}}_{en}^{\mathrm{trial}}\Big)\Big]\,\boldsymbol{n}_n = \|\boldsymbol{s}_n^{\mathrm{trial}}\|\boldsymbol{n}_n^{\mathrm{trial}}. \tag{45}$$

Since the sum in brackets on the left-hand-side of (45) is a non-negative scalar, the tensors $\boldsymbol{n}_n$ and $\boldsymbol{n}_n^{\mathrm{trial}}$ are parallel to each other, and, since they also have the same norm, it must hold that $\boldsymbol{n}_n = \boldsymbol{n}_n^{\mathrm{trial}}$. Therefore, equation (45) also implies the equalities

$$\boldsymbol{s}_n = \boldsymbol{s}_n^{\mathrm{trial}} - \tfrac{2}{3}\mu\gamma_{\tau n}\Delta t_n \mathrm{tr}\Big(\boldsymbol{g}\,\overline{\boldsymbol{b}}_{en}^{\mathrm{trial}}\Big)\,\boldsymbol{n}_n^{\mathrm{trial}}, \tag{46a}$$

$$\|\boldsymbol{s}_n\| = \|\boldsymbol{s}_n^{\mathrm{trial}}\| - \tfrac{2}{3}\mu\gamma_{\tau n}\Delta t_n \mathrm{tr}\Big(\boldsymbol{g}\,\overline{\boldsymbol{b}}_{en}^{\mathrm{trial}}\Big). \tag{46b}$$

Equation (46a) is the time-discrete flow rule (43) written in terms of stress, while, through the introduction of the yield functions

$$f_{\tau n} := \|\boldsymbol{s}_n\| - \sqrt{\tfrac{2}{3}}\Big(K(\alpha_n) + \tau_y\Big), \tag{47a}$$

$$f_{\tau n}^{\mathrm{trial}} := \|\boldsymbol{s}_n^{\mathrm{trial}}\| - \sqrt{\tfrac{2}{3}}\Big(K(\alpha_{n-1}) + \tau_y\Big), \tag{47b}$$

equation (46b) can be rephrased as

$$f_{\tau n} = f_{\tau n}^{\mathrm{trial}} - \tfrac{2}{3}\mu\gamma_{\tau n}\Delta t_n \mathrm{tr}\Big(\boldsymbol{g}\,\overline{\boldsymbol{b}}_{en}^{\mathrm{trial}}\Big) - \sqrt{\tfrac{2}{3}}\Big(K(\alpha_n) - K(\alpha_{n-1})\Big). \tag{48}$$

Consequently, the condition that plastic flow occurs at time t_n, obtained by setting $f_{\tau n} = 0$, is transformed into an equation that defines $\gamma_{\tau n}$ implicitly [15]:

$$\tfrac{2}{3}\mu\gamma_{\tau n}\Delta t_n \mathrm{tr}\Big(\boldsymbol{g}\,\overline{\boldsymbol{b}}_{en}^{\mathrm{trial}}\Big) + \sqrt{\tfrac{2}{3}}\Big(K\Big(\alpha_{n-1} + \sqrt{\tfrac{2}{3}}\gamma_{\tau n}\Delta t_n\Big) - K(\alpha_{n-1})\Big) = f_{\tau n}^{\mathrm{trial}}. \tag{49}$$

In (49), $f_{\tau n}^{\mathrm{trial}}$ is regarded as known, and the time-discrete version of (35c) has been used to express α_n as a function of α_{n-1} and $\gamma_{\tau n}$. When the condition $f_{\tau n}^{\mathrm{trial}} \le 0$ applies, $\gamma_{\tau n} = 0$. In the case of non-linear hardening, (49) is non-linear too, and is solved numerically (e.g. by means of the Newton method). For linear hardening, $\hat{\mathfrak{H}}_\kappa$ is quadratic in α, and one obtains [15]

$$\gamma_{\tau n}\Delta t_n = \begin{cases} \frac{f_{\tau n}^{\mathrm{trial}}}{\frac{2}{3}\mu\mathrm{tr}(\boldsymbol{g}\overline{\boldsymbol{b}}_{en}^{\mathrm{trial}}) + \frac{2}{3}H}, & \text{if } f_{\tau n}^{\mathrm{trial}} > 0, \\ 0, & \text{if } f_{\tau n}^{\mathrm{trial}} \le 0, \end{cases} \tag{50}$$

where H is a constant material parameter having the same units as μ and defined by

$$H = \frac{\partial K}{\partial \alpha}(\alpha) = \frac{\partial^2 \hat{\mathfrak{H}}_\kappa}{\partial \alpha^2}(\alpha). \tag{51}$$

Both (49) and (50) determine $\gamma_{\tau n}$ as a function of $\boldsymbol{F}_n$ (or, equivalently, as a functional of χ_n). Moreover, once $\gamma_{\tau n}$ is computed, α_n is obtained by $\alpha_n = \alpha_{n-1} + \sqrt{\frac{2}{3}}\gamma_{\tau n}\Delta t_n$, which is the time-discrete version of (35c). This decouples (35c) from (35a) and (35b).

The most important consequence of the assumptions discussed in this section is that, since $\boldsymbol{n}_n = \boldsymbol{n}_n^{\text{trial}}$ and $\text{tr}(\boldsymbol{g}\bar{\boldsymbol{b}}_{\text{e}n}) = \text{tr}(\boldsymbol{g}\bar{\boldsymbol{b}}_{\text{e}n}^{\text{trial}}) = \text{tr}(\boldsymbol{B}_{\text{p}(n-1)}\boldsymbol{C}_n)$, and none of these quantities depends on $\boldsymbol{B}_{\text{p}n}$, the flow rule (43) allows to express $\boldsymbol{B}_{\text{p}n}$ as a non-linear function of χ_n:

$$\boldsymbol{B}_{\text{p}n} = \hat{\boldsymbol{B}}_{\text{p}n}(\chi_n) := \boldsymbol{B}_{\text{p}(n-1)} - \tfrac{2}{3}\Delta t_n \gamma_{\tau n}(\chi_n)\text{tr}(\boldsymbol{B}_{\text{p}(n-1)}\boldsymbol{C}_n)\boldsymbol{F}_n^{-1}\boldsymbol{n}_n^{\text{trial}}\boldsymbol{F}_n^{-\text{T}}, \tag{52}$$

with $\gamma_{\tau n}(\chi_n) > 0$. Here, it holds that $\boldsymbol{C}_n = \boldsymbol{F}_n^{\text{T}}\boldsymbol{g}\boldsymbol{F}_n$.

5.2 Time-Discrete Setting

By performing a backward Euler method in time, the results obtained in section 5.1 allow to reformulate the problem 'Pr1' as follows:

Given the initial data $\boldsymbol{B}_{\text{p}0}(X)$ and $\alpha_0(X)$ for all $X \in \mathcal{B}$, and the Dirichlet-boundary condition $\chi_{\text{b}n}(X)$ for all $X \in \partial\mathcal{B}_{\text{D}}$, find $\chi_n \in \big(H^1(\mathcal{B}, \mathcal{S})\big)^3$, $\boldsymbol{B}_{\text{p}n} \in \mathbf{L}^2(\mathcal{B}, T\mathcal{B} \otimes T\mathcal{B})$ and $\alpha_n \in L^2(\mathcal{B}, \mathbb{R})$ such that $\chi_n = \chi_{\text{b}n}$, for all $n \geq 0$ and $X \in \partial\mathcal{B}_{\text{D}}$ and, for all $n \geq 1$,

$$\boldsymbol{B}_{\text{p}n} = \begin{cases} \boldsymbol{B}_{\text{p}(n-1)}, & \text{if } \gamma_{\tau n} = 0, \\ \hat{\boldsymbol{B}}_{\text{p}n}(\chi_n) = \boldsymbol{B}_{\text{p}(n-1)} - \hat{\boldsymbol{\mathfrak{R}}}_n(\chi_n), & \text{if } \gamma_{\tau n} > 0, \end{cases} \tag{53a}$$

$$\alpha_n = \begin{cases} \alpha_{n-1}, & \text{if } \gamma_{\tau n} = 0, \\ \alpha_{n-1} + \sqrt{\tfrac{2}{3}}\gamma_{\tau n}(\chi_n)\Delta t_n, & \text{if } \gamma_{\tau n} > 0, \end{cases} \tag{53b}$$

$$\mathcal{P}'(\chi_n, \tilde{\boldsymbol{u}}) = \begin{cases} \int_{\mathcal{B}} \hat{\boldsymbol{P}}\big(\chi_n, \boldsymbol{B}_{\text{p}(n-1)}\big) : \boldsymbol{g}\text{Grad}\tilde{\boldsymbol{u}} = 0, & \text{if } \gamma_{\tau n} = 0, \\ \int_{\mathcal{B}} \hat{\boldsymbol{P}}\Big(\chi_n, \hat{\boldsymbol{B}}_{\text{p}n}(\chi_n)\Big) : \boldsymbol{g}\text{Grad}\tilde{\boldsymbol{u}} = 0, & \text{if } \gamma_{\tau n} > 0, \end{cases} \tag{53c}$$

where (53c) has to hold for all $\tilde{\boldsymbol{u}} \in \tilde{\mathcal{H}}$, $\gamma_{\tau n}(\chi_n)$ is determined either by (49) or by (50), and $\hat{\boldsymbol{\mathfrak{R}}}_n(\chi_n)$ is defined as

$$\hat{\boldsymbol{\mathfrak{R}}}_n(\chi_n) = \tfrac{2}{3}\Delta t_n \gamma_{\tau n}(\chi_n)\text{tr}(\boldsymbol{B}_{\text{p}(n-1)}\boldsymbol{C}_n)\boldsymbol{F}_n^{-1}\boldsymbol{n}_n^{\text{trial}}\boldsymbol{F}_n^{-\text{T}}. \tag{54}$$

The functional $\mathcal{P}'(\chi_n, \tilde{\boldsymbol{u}})$ is non-linear in χ_n regardless of whether $\gamma_{\tau n}$ is zero or positive. This is because the first Piola-Kirchhoff stress tensor is a non-linear constitutive functional of χ_n within the framework of finite deformations. Thus, iterative procedures (e.g. Newton method) are required to solve (53c). Note that the formulation of the RMA summarised above, which leads to (52) and (54), is such that $\boldsymbol{B}_{\text{p}n}$ can be expressed as an explicit function of χ_n. In other words, the time-discrete flow rule (52) can be rewritten as

$$\mathfrak{G}_n(\chi_n, \boldsymbol{B}_{\text{p}n}) = \boldsymbol{B}_{\text{p}n} - \boldsymbol{B}_{\text{p}(n-1)} + \hat{\boldsymbol{\mathfrak{R}}}_n(\chi_n) = \boldsymbol{0}, \tag{55}$$

with $\mathfrak{G}_n$ being non-linear in χ_n and affine in $\boldsymbol{B}_{\text{p}n}$. Consequently, no linearisation of the flow rule with respect to $\boldsymbol{B}_{\text{p}n}$ is necessary. However, this simplification cannot be done if the assumptions discussed in Section 5 (decoupling of the strain energy density function as in (39), and approximation of the flow rule as in (40)) cannot be invoked. For example, this can be the case described in 'Pr2', where no hypotheses are done on the right-hand-side of (38b). This motivates the study of problems of the same type as 'Pr2' by means of the Generalised Plasticity Algorithm (GPA) proposed in this paper.

By using numerical quadrature rules within Finite Element Methods, the equations (49), (53a), (53b) and (54), are evaluated at the integration points of every finite element of the spatial discretisation of the problem.

Although this work does use the assumption of isotropy, the proposed algorithm does not invoke an approximation of the flow rule. This has the repercussions that the plastic

variable $\boldsymbol{B}_{\mathrm{p}n}$ cannot be rewritten as a function of the deformation χ_n, and, consequently, the flow rule cannot be decoupled from the balance of momentum. Rather, $\boldsymbol{B}_{\mathrm{p}n}$ has to be regarded as an unknown having, at least in principle, the same 'dignity' as χ_n. If, on the one hand, this complicates the numerical treatment of the elastoplastic problem, on the other hand, it makes the computational algorithm more flexible and appliable also to those cases, which do not require that $\boldsymbol{n}_n^{\mathrm{trial}}$ is equal to $\boldsymbol{n}_n$. The proposed method is presented in detail in section 6.

6 Discretisation and Linearisation of the Problem 'Pr2'

The discrete, linearised version of the problem 'Pr2' (cf. (37)–(38b)) is constructed in three steps. Firstly, a backward Euler method is used for discretising the flow rule (38b). Secondly, the time-discrete version of (38) is put in a form suitable for Finite Element analysis. Thirdly, the Finite Element Method is employed for the discretisation in space.

6.1 The Generalised Plasticity Algorithm (GPA)

The time-discrete version of the problem 'Pr2' can be formulated as follows:

Find $\chi_n \in \left(H^1(\mathcal{B},\mathcal{S})\right)^3$ and $\boldsymbol{B}_{\mathrm{p}n} \in \mathbf{L}^2(\mathcal{B}, T\mathcal{B}\otimes T\mathcal{B})$ such that $\chi_n = \chi_{\mathrm{b}n}$, for all $n \geq 0$ and $X \in \partial\mathcal{B}_{\mathrm{D}}$ and, for all $n \geq 1$,

$$\mathcal{P}(\chi_n, \boldsymbol{B}_{\mathrm{p}n}, \tilde{\boldsymbol{u}}) := \int_{\mathcal{B}} \hat{\boldsymbol{P}}(\chi_n, \boldsymbol{B}_{\mathrm{p}n}) : \boldsymbol{g}\mathrm{Grad}\,\tilde{\boldsymbol{u}} = 0, \qquad \forall\ \tilde{\boldsymbol{u}} \in \tilde{\mathcal{H}}, \tag{56a}$$

$$\mathcal{G}(\chi_n, \boldsymbol{B}_{\mathrm{p}n}) = \boldsymbol{B}_{\mathrm{p}n} - \boldsymbol{B}_{\mathrm{p}(n-1)} + \hat{\boldsymbol{\mathcal{R}}}_n(\chi_n, \boldsymbol{B}_{\mathrm{p}n}) = \boldsymbol{0}, \quad \boldsymbol{B}_{\mathrm{p}}(X,0) = \boldsymbol{B}_{\mathrm{p}0}(X) \text{ in } \mathcal{B}. \tag{56b}$$

Equations (56) are generally highly non-linear and coupled with each other. To search for solutions, (56a) and (56b) are linearised at each time step in a two-stage fashion according to Newton's method. At the kth and lth iteration, $\chi_{n,k}$ and $\boldsymbol{B}_{\mathrm{p}n,l}$ are written as

$$\chi_{n,k} = \chi_{n,k-1} + \boldsymbol{h}_{n,k}, \qquad \boldsymbol{B}_{\mathrm{p}n,l} = \boldsymbol{B}_{\mathrm{p}n,l-1} + \boldsymbol{\Phi}_{n,l}\,, \quad k,l \geq 1, \tag{57}$$

where $\boldsymbol{h}_{n,k}$ and $\boldsymbol{\Phi}_{n,l}$ are the increments associated with χ_n and $\boldsymbol{B}_{\mathrm{p}n}$, respectively. Thus, one can regard the deformation gradient tensor as a functional of the motion and write $\boldsymbol{F}_{n,k} = \boldsymbol{F}(\chi_{n,k})$ and $\boldsymbol{F}_{n,k-1} = \boldsymbol{F}(\chi_{n,k-1})$ as well as $\boldsymbol{H}_{n,k} = D_\chi \boldsymbol{F}_{n,k-1}[\boldsymbol{h}_{n,k}]$, the latter being the Gâteaux-derivative of the functional $\boldsymbol{F}$ with respect to the motion, evaluated at $\chi_{n,k-1}$, and computed along the increment $\boldsymbol{h}_{n,k}$. It follows that $D_\chi \boldsymbol{F}_{n,k-1}[\boldsymbol{h}_{n,k}] = \mathrm{Grad}\boldsymbol{h}_{n,k}$.

To describe the linearisation procedure in detail, it is useful to introduce the notation

$$D_\chi \mathcal{P}(\chi_{n,k-1}, \boldsymbol{B}_{\mathrm{p}n}, \tilde{\boldsymbol{u}})[\boldsymbol{h}_{n,k}] = \int_{\mathcal{B}} \boldsymbol{g}\mathrm{Grad}\tilde{\boldsymbol{u}} : \mathbb{A}(\chi_{n,k-1}, \boldsymbol{B}_{\mathrm{p}n}) : \boldsymbol{H}_{n,k}\,, \tag{58a}$$

$$D_{\boldsymbol{B}_{\mathrm{p}}} \mathcal{P}(\chi_n, \boldsymbol{B}_{\mathrm{p}n,l-1}, \tilde{\boldsymbol{u}})[\boldsymbol{\Phi}_{n,l}] = \int_{\mathcal{B}} \boldsymbol{g}\mathrm{Grad}\tilde{\boldsymbol{u}} : \mathbb{B}(\chi_n, \boldsymbol{B}_{\mathrm{p}n,l-1}) : \boldsymbol{\Phi}_{n,l}\,, \tag{58b}$$

$$D_{\boldsymbol{B}_{\mathrm{p}}} \mathcal{G}(\chi_n, \boldsymbol{B}_{\mathrm{p}n,l-1})[\boldsymbol{\Phi}_{n,l}] = \mathbb{Y}(\chi_n, \boldsymbol{B}_{\mathrm{p}n,l-1}) : \boldsymbol{\Phi}_{n,l}\,, \tag{58c}$$

with

$$\mathbb{A}(\chi_{n,k-1}, \boldsymbol{B}_{\mathrm{p}n}) : \boldsymbol{H}_{n,k} = D_\chi \hat{\boldsymbol{P}}(\chi_{n,k-1}, \boldsymbol{B}_{\mathrm{p}n})[\boldsymbol{h}_{n,k}]\,, \tag{59a}$$

$$\mathbb{B}(\chi_n, \boldsymbol{B}_{\mathrm{p}n,l-1}) : \boldsymbol{\Phi}_{n,l} = D_{\boldsymbol{B}_{\mathrm{p}}} \hat{\boldsymbol{P}}(\chi_n, \boldsymbol{B}_{\mathrm{p}n,l-1})[\boldsymbol{\Phi}_{n,l}]\,. \tag{59b}$$

The fourth-order tensor $\mathbb{A}$ is the algorithmic acoustic tensor. The expressions defining explicitly $\mathbb{A}$, $\mathbb{B}$ and $\mathbb{Y}$ depend strongly on the constitutive model and on the flow rule.

The first stage of the GPA consists of linearising (56a) and (56b) with respect to $\boldsymbol{B}_{\mathrm{p}}$ only. This defines two approximated expressions of $\mathcal{P}$ and $\mathcal{G}$ that read at the lth iteration

$$\Delta_{\mathcal{P}} := \mathcal{P}(\chi_n, \boldsymbol{B}_{\mathrm{p}n,l-1}, \tilde{\boldsymbol{u}}) + D_{\boldsymbol{B}_{\mathrm{p}}}\mathcal{P}(\chi_n, \boldsymbol{B}_{\mathrm{p}n,l-1}, \tilde{\boldsymbol{u}})[\boldsymbol{\Phi}_{n,l}]\,, \tag{60a}$$

$$\boldsymbol{\Delta}_{\mathcal{G}} := \mathcal{G}(\chi_n, \boldsymbol{B}_{\mathrm{p}n,l-1}) + \mathbb{Y}(\chi_n, \boldsymbol{B}_{\mathrm{p}n,l-1}) : \boldsymbol{\Phi}_{n,l}\,. \tag{60b}$$

Note that $\Delta_{\mathcal{P}}$ and $\boldsymbol{\Delta}_{\mathcal{G}}$ are, respectively, a scalar and a second-order tensor since they are obtained by linearising the internal virtual power and the flow rule.

The dependence of $\mathcal{G}$ on $\boldsymbol{B}_{\mathrm{p}n}$ (cf. (56b)) is such that $\mathbb{Y}$ is invertible. Therefore, the increment $\boldsymbol{\Phi}_{n,l}$ can be expressed as a function of χ_n by setting (60b) equal to zero, i.e.

$$\boldsymbol{\Phi}_{n,l} = -[\mathbb{Y}(\chi_n, \boldsymbol{B}_{\mathrm{p}n,l-1})]^{-1} : \mathcal{G}(\chi_n, \boldsymbol{B}_{\mathrm{p}n,l-1}). \tag{61}$$

By substituting the right-hand-side of (61) into (60a), $\boldsymbol{\Phi}_{n,l}$ is eliminated statically from $\Delta_{\mathcal{P}}$ (this is similar to an algorithm of Gauß-Seidel type), which becomes

$$\Delta_{\mathcal{P}} = \mathcal{P}(\chi_n, \boldsymbol{B}_{\mathrm{p}n,l-1}, \tilde{\boldsymbol{u}}) - D_{\boldsymbol{B}_{\mathrm{p}}}\mathcal{P}(\chi_n, \boldsymbol{B}_{\mathrm{p}n,l-1}, \tilde{\boldsymbol{u}}) \left[[\mathbb{Y}(\chi_n, \boldsymbol{B}_{\mathrm{p}n,l-1})]^{-1} : \mathcal{G}(\chi_n, \boldsymbol{B}_{\mathrm{p}n,l-1})\right]. \tag{62}$$

At each time step, the motion χ_n is required to solve the equation $\Delta_{\mathcal{P}} = 0$. However, $\Delta_{\mathcal{P}}$ is defined in (62) as a highly non-linear functional of χ_n, $\Delta_{\mathcal{P}} \equiv \Delta_{\mathcal{P}}(\chi_n, \boldsymbol{B}_{\mathrm{p}n,l-1}, \tilde{\boldsymbol{u}})$. The second stage of the GPA consists, thus, of linearising $\Delta_{\mathcal{P}}$ with respect to χ_n, and setting equal to zero its linearised expression. At the kth iteration of this linearisation sub-procedure, one has to solve

$$\Delta_{\mathcal{P}}(\chi_{n,k-1}, \boldsymbol{B}_{\mathrm{p}n,l-1}, \tilde{\boldsymbol{u}}) + D_{\chi}\Delta_{\mathcal{P}}(\chi_{n,k-1}, \boldsymbol{B}_{\mathrm{p}n,l-1}, \tilde{\boldsymbol{u}})[\boldsymbol{h}_{n,k}] = 0\,. \tag{63}$$

By introducing the auxiliary functional

$$g(\chi_n, \boldsymbol{B}_{\mathrm{p}n,l-1}, \tilde{\boldsymbol{u}}) := D_{\boldsymbol{B}_{\mathrm{p}}}\mathcal{P}(\chi_n, \boldsymbol{B}_{\mathrm{p}n,l-1}, \tilde{\boldsymbol{u}}) \left[[\mathbb{Y}(\chi_n, \boldsymbol{B}_{\mathrm{p}n,l-1})]^{-1} : \mathcal{G}(\chi_n, \boldsymbol{B}_{\mathrm{p}n,l-1})\right], \tag{64}$$

$\Delta_{\mathcal{P}}$ becomes

$$\Delta_{\mathcal{P}}(\chi_n, \boldsymbol{B}_{\mathrm{p}n,l-1}, \tilde{\boldsymbol{u}}) = \mathcal{P}(\chi_n, \boldsymbol{B}_{\mathrm{p}n,l-1}, \tilde{\boldsymbol{u}}) - g(\chi_n, \boldsymbol{B}_{\mathrm{p}n,l-1}, \tilde{\boldsymbol{u}})\,, \tag{65}$$

and (63) can be rewritten as

$$\begin{aligned} &\Delta_{\mathcal{P}}(\chi_{n,k-1}, \boldsymbol{B}_{\mathrm{p}n,l-1}, \tilde{\boldsymbol{u}}) \\ &+ D_{\chi}\mathcal{P}(\chi_{n,k-1}, \boldsymbol{B}_{\mathrm{p}n,l-1}, \tilde{\boldsymbol{u}})[\boldsymbol{h}_{n,k}] - D_{\chi}g(\chi_{n,k-1}, \boldsymbol{B}_{\mathrm{p}n,l-1}, \tilde{\boldsymbol{u}})[\boldsymbol{h}_{n,k}] = 0\,. \end{aligned} \tag{66}$$

The Gâteaux-derivative of g can be expressed by means of a fourth-order tensor $\mathbb{A}'$ such that

$$D_{\chi}g(\chi_{n,k-1}, \boldsymbol{B}_{\mathrm{p}n,l-1}, \tilde{\boldsymbol{u}})[\boldsymbol{h}_{n,k}] = \int_{\mathcal{B}} \boldsymbol{g}\mathrm{Grad}\tilde{\boldsymbol{u}} : \mathbb{A}'(\chi_{n,k-1}, \boldsymbol{B}_{\mathrm{p}n,l-1}) : \boldsymbol{H}_{n,k}\,, \tag{67}$$

which, by using (58a), allows to reformulate (66) as follows

Find $\boldsymbol{h}_{n,k} \in \left(H_0^1(\mathcal{B}, T\mathcal{S})\right)^3$ such that, for all $n \geq 1$ and $k \geq 1$,

$$\overline{c}(\boldsymbol{h}_{n,k}, \tilde{\boldsymbol{u}}) = \overline{g}(\tilde{\boldsymbol{u}}), \quad \forall\ \tilde{\boldsymbol{u}} \in \left(H_0^1(\mathcal{B}, T\mathcal{S})\right)^3\,, \tag{68}$$

where

$$\overline{c}(\boldsymbol{h}_{n,k},\tilde{\boldsymbol{u}}) := \int_{\mathcal{B}} \boldsymbol{g}\mathrm{Grad}\tilde{\boldsymbol{u}} : \overline{\mathbb{A}}_{n,k-1,l-1} : \mathrm{Grad}\boldsymbol{h}_{n,k}, \tag{69a}$$

$$\overline{\mathbb{A}}_{n,k-1,l-1} := \mathbb{A}_{n,k-1,l-1} - \mathbb{A}'_{n,k-1,l-1}, \tag{69b}$$

$$\begin{aligned}\overline{g}(\tilde{\boldsymbol{u}}) &:= -\mathcal{P}(\chi_{n,k-1},\boldsymbol{B}_{\mathrm{p}n,l-1},\tilde{\boldsymbol{u}}) \\ &\quad + \int_{\mathcal{B}} \boldsymbol{g}\mathrm{Grad}\tilde{\boldsymbol{u}} : \left(\mathbb{B}_{n,k-1,l-1} : \mathbb{Y}^{-1}_{n,k-1,l-1}\right) : \mathcal{G}_{n,k-1,l-1}\,,\end{aligned} \tag{69c}$$

and the notation $\mathbb{A}_{n,k-1,l-1} = \mathbb{A}(\chi_{n,k-1},\boldsymbol{B}_{\mathrm{p}n,l-1})$, $\mathbb{B}_{n,k-1,l-1} = \mathbb{B}(\chi_{n,k-1},\boldsymbol{B}_{\mathrm{p}n,l-1})$, and $\mathbb{Y}_{n,k-1,l-1} = \mathbb{Y}(\chi_{n,k-1},\boldsymbol{B}_{\mathrm{p}n,l-1})$ has been used. The increments $\boldsymbol{h}_{n,k}$ belong, for all n and for all k, to the same functional space as the test velocities, i.e. $\boldsymbol{h}_{n,k}$ must vanish on $\partial\mathcal{B}_{\mathrm{D}}$ since, at each iteration and each time, the motion must comply with χ_{b}.

The tangent operator $\overline{\mathbb{A}}_{n,k-1,l-1}$ has been calculated by determining the numerical derivative of the right-hand-side of the functional $\Delta_{\mathcal{P}}$ (cf. (65)) with respect to the motion χ_n. This is because the explicit expression of g in (64) is very cumbersome.

6.2 Fully Discrete Linearised Setting

Let then $\mathscr{T}$ be a regular triangularisation of $\mathrm{Cl}(\mathcal{B}) = \mathcal{B}\cup\partial\mathcal{B}$ —the closure of $\mathcal{B}$— in N^h non-overlapping elements $\{T_i\}_{i=1}^{N^h}$, where $h>0$ is the grid characteristic length. Moreover, let $\mathbb{P}_m(T_i)$ be the space of polynomials of order m over T_i, for all $i=1,\dots,N^h$. Hence, setting for ease of notation $\mathscr{V}\equiv\left(H^1_0(\mathcal{B},\mathcal{S})\right)^3$, the following linear finite element space is introduced

$$\mathscr{V}^h_m := \{\tilde{\boldsymbol{u}}^h\in\mathscr{V}\ :\ \tilde{\boldsymbol{u}}^h_{|T_i}\in(\mathbb{P}_m(T_i))^3\,,\ \forall\, T_i\in\mathscr{T},\ \ \tilde{\boldsymbol{u}}^h_{|\partial\mathcal{B}_{\mathrm{D}}}=\boldsymbol{0}\}\,, \tag{70}$$

where the notation $(\mathbb{P}_m(T_i))^3$ means that each component of the vector-valued function $\tilde{\boldsymbol{u}}^h_{|T_i}$, restriction of $\tilde{\boldsymbol{u}}^h$ to the element T_i, is a polynomial of degree m (in the following, m will be either 1 or 2). The space $\mathscr{V}^h_m$ is spanned by the Lagrangian basis functions $\{\boldsymbol{\varphi}^q\}_{q=1}^M$, with $M=\dim(\mathscr{V}^h_m)$, so that the approximations of the test velocity $\tilde{\boldsymbol{u}}$ and of the increment $\boldsymbol{h}_{n,k}$ can be written, at each time t_n and at each Newton iteration step k, as

$$\tilde{\boldsymbol{u}}^h = \sum_{q=1}^M \tilde{u}^q\boldsymbol{\varphi}^q, \qquad \boldsymbol{h}^h_{n,k} = \sum_{q=1}^M h^q_{n,k}\boldsymbol{\varphi}^q \in \mathscr{V}^h_m. \tag{71}$$

The approximation of $\chi_{n,k}\in\mathcal{H}$ is constructed as in (57). At each time t_n, the sequence $\{\chi^h_{n,k}\}_{k\in\mathbb{N}}$ is contained in the set $\mathcal{H}^h\subset\mathcal{H}$ defined by

$$\mathcal{H}^h := \{\chi^h_n\in\mathcal{H}\ :\ \chi^h_{n\,|\partial\mathcal{B}_{\mathrm{D}}} = \chi^h_{\mathrm{b}n}\}, \tag{72}$$

where $\chi^h_{\mathrm{b}n}$ is the approximation of the boundary data χ_{b} at time t_n. The approximated motion $\chi^h_{n,k-1}$, used to determine the right-hand-side of (57), is written as

$$\chi^h_{n,k-1} = y^h_n + \boldsymbol{h}^h_{n,k-1} \tag{73}$$

with $\boldsymbol{h}^h_{n,k-1}\in\mathscr{V}^h_m$ and $y^h_{n\,|\partial\mathcal{B}_{\mathrm{D}}} = \chi^h_{\mathrm{b}n}$. Finally, the finite element version of (68) becomes:

Find $\boldsymbol{h}^h_{n,k}\in\mathscr{V}^h_m$ such that, for all $n\geq 1$ and $k\geq 1$,

$$\overline{c}(\boldsymbol{h}^h_{n,k},\boldsymbol{\varphi}^q) = \overline{g}(\boldsymbol{\varphi}^q), \quad \forall\ q=1,\dots,M\,. \tag{74}$$

The integrals featuring in $\overline{c}(\,\cdot\,,\,\cdot\,)$ and $\overline{g}(\,\cdot\,)$ are approximated by numerical quadrature.

7 Numerical Tests and Results

Due to the high non-linearity of the considered problems, the load attributed via the Dirichlet boundary conditions is applied incrementally. This leads to better starting values for the Newton method in every incremental step. Moreover, a line search method is applied to ensure global convergence of the non-linear iterations.

7.1 Comparison with the RMA for a Shear-Compression Test

As a first benchmark for evaluating the implementation of the GPA, and comparing it with the RMA, the shear-compression test of a unit cube presented in [56] is investigated. The unit cube is made of a material that is assumed to exhibit perfect plastic behaviour, i.e. no hardening is considered. Thus, the energy densities $\hat{\psi}_\kappa$ and $\hat{W}_\kappa$ differ from each other additively by a constant (cf. (14)), q vanishes identically (cf. (15c)), and the model is described by $\hat{W}_\kappa$ (cf. (39)) and the yield function $f_\tau(\boldsymbol{\tau}_\kappa) = \|\mathrm{dev}(\boldsymbol{\tau}_\kappa)\| - \sqrt{(2/3)}\tau_y$. Moreover, since $q = -K(\alpha) = 0$, equation (49) delivers

$$\gamma_{\tau n}\Delta t_n = \begin{cases} \frac{f_{\tau n}^{\mathrm{trial}}}{\frac{2}{3}\mu \mathrm{tr}(\boldsymbol{g}\bar{\boldsymbol{b}}_{\mathrm{e}n}^{\mathrm{trial}})}, & \text{if } f_{\tau n}^{\mathrm{trial}} > 0, \\ 0, & \text{if } f_{\tau n}^{\mathrm{trial}} \leq 0. \end{cases} \tag{75}$$

In an orthonormal Cartesian reference frame, the Dirichlet boundary conditions can be written as follows: For all $t \in \mathcal{I} \equiv [0, T]$,

$$\chi_{\mathrm{b}}^1(X,t) = X^1 + 0.3\frac{t}{T}, \quad \chi_{\mathrm{b}}^2(X,t) = X^2 - 0.3\frac{t}{T}, \quad \chi_{\mathrm{b}}^3(X,t) = X^3, \quad \text{on } [X^1, 1, X^3], \tag{76a}$$

$$\chi_{\mathrm{b}}^1(X,t) = X^1, \quad \chi_{\mathrm{b}}^2(X,t) = X^2, \quad \chi_{\mathrm{b}}^3(X,t) = X^3, \quad \text{on } [X^1, 0, X^3], \tag{76b}$$

with $[X^1, 1, X^3] = [0,1] \times \{1\} \times [0,1]$, $[X^1, 0, X^3] = [0,1] \times \{0\} \times [0,1]$. The conditions (76) describe a cube clamped at the bottom surface, $X^2 = 0$, and undergoing shear and compression at the top surface $X^2 = 1$ with a deformation up to 30%. The material parameters used for this test are reported in Table 1 (even though hardening is not considered in this example, the material parameters H_∞, H, and ω are reported in Table 1, since they shall be used in next benchmarks). Note that the parameters reported in Table 1 are taken from [15], and model the material behaviour of steel (cf. [6]).

Table 1: Material parameters

bulk modulus	κ	$164206.00\,\mathrm{N/mm^2}$
shear modulus	μ	$80193.80\,\mathrm{N/mm^2}$
initial yield stress	τ_y	$450.00\,\mathrm{N/mm^2}$
saturation stress	H_∞	$715.00\,\mathrm{N/mm^2}$
linear hardening modulus	H	$129.24\,\mathrm{N/mm^2}$
hardening exponent	ω	16.93

To check whether the GPA (cf. Section 6.1) produces results comparable with the RMA, the maximal eigenvalue of the Kirchhoff stress tensor $\boldsymbol{\tau}_\kappa$ at the midpoint of the unit cube is computed (see Fig. 1). Both the RMA and the GPA determine the same results. In Figure 1, the deformation of the cube in the shear-compression test is shown at time $t = T = 300$ s. Moreover, in Table 2, the computed values of the invariants of the Mandel stress tensor $\boldsymbol{\Sigma}$ are reported for different deformations.

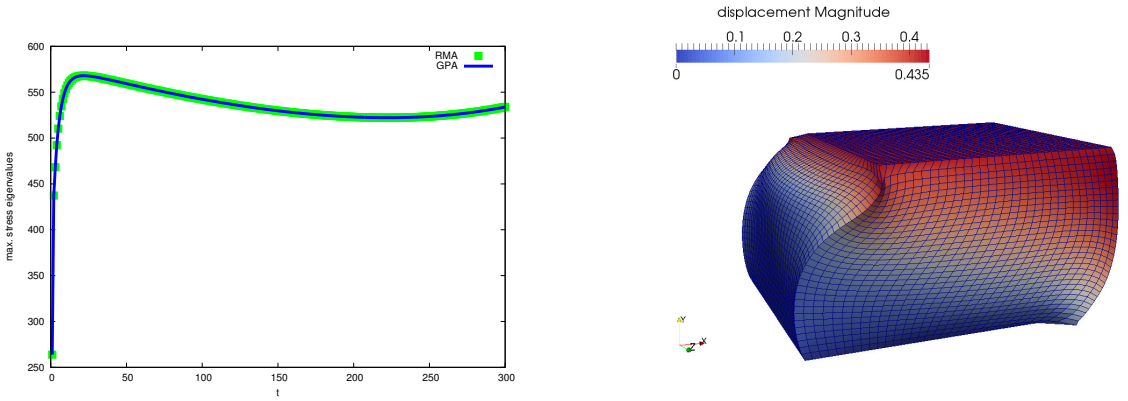

Figure 1: (Left) Maximal eigenvalue of $\boldsymbol{\tau}_\kappa$ at $X = (0.5, 0.5, 0.5)$ using the 'RMA' (green) and the 'GPA' (blue) with $T = 300$ s. (Right) Deformation of the unit cube in a shear compression test at $t = T = 300$ s.

Table 2: Comparison of the invariants of the Mandel stress tensor at $t = T/300$, $t = T/3$ and $t = T$, which correspond to deformations of 0.1%, 10% and 30%, respectively. The models M1, M2, M3, M4, M5 can be found in [56]. In the present paper, computations have been run with a modified version of model M4, which is referred to $\widetilde{\text{M4}}$ hereafter, while the results shown in [56] are taken as reference for comparisons. $\widetilde{\text{M4}}$ combines the energy potential of the model M4 [56], with the flow rule (40). The deformation at $t = T/300$ serves to check for non-linear elasticity, since no plastic strains occur.

	M1(10%)	M1(30%)	M2(10%)	M2(30%)	$\widetilde{\textbf{M4}}$(10%)	$\widetilde{\textbf{M4}}$(30%)
$\bar{I}_1(\boldsymbol{\Sigma})$	-9.485_{+02}	-9.977_{+02}	-9.251_{+02}	-9.190_{+02}	-9.218_{+02}	-9.141_{+02}
$\bar{I}_2(\boldsymbol{\Sigma})$	1.984_{+05}	2.257_{+05}	1.840_{+05}	1.803_{+05}	1.826_{+05}	1.786_{+05}
$\bar{I}_3(\boldsymbol{\Sigma})$	-1.161_{+07}	-1.473_{+07}	-1.013_{+07}	-9.936_{+06}	-1.002_{+07}	-9.944_{+06}
	M2(0.1%)	M3(0.1%)	M4(0.1%)	M5(0.1%)	$\widetilde{\textbf{M4}}$(0.1%)	
$\bar{I}_1(\boldsymbol{\Sigma})$	-2.557_{+02}	-2.550_{+02}	-2.560_{+02}	-2.563_{+02}	-2.560_{+02}	
$\bar{I}_2(\boldsymbol{\Sigma})$	-2.205_{+03}	-2.253_{+03}	-2.207_{+03}	-2.210_{+03}	-2.213_{+03}	
$\bar{I}_3(\boldsymbol{\Sigma})$	3.228_{+04}	3.201_{+04}	3.232_{+04}	3.235_{+04}	3.232_{+04}	

7.1.1 Structural Set-Up

RMA: Let $\boldsymbol{P}_n = \hat{\boldsymbol{P}}(\chi_n, \boldsymbol{B}_{\text{p}n})$ be the stress response defined by computing $\boldsymbol{B}_{\text{p}n}$ as prescribed by (52) and substituting the result into the time-discrete version of the constitutive expression of $\boldsymbol{P}$ (37). As stated in Section 5.2, $\mathcal{P}'(\chi_n, \tilde{\boldsymbol{u}})$ is non-linear in χ_n. Therefore, an iterative scheme has to be applied to determine χ_n at each time step. Let then $\chi_{n,k} = \chi_{n,k-1} + \boldsymbol{h}_{n,k}$, $k \geq 1$, be the motion at the kth Newton iteration, where the increment $\boldsymbol{h}_{n,k}$ solves the linearised equation

$$\mathcal{P}'(\chi_{n,k-1}, \tilde{\boldsymbol{u}}) + D_\chi \mathcal{P}'(\chi_{n,k-1}, \tilde{\boldsymbol{u}})[\boldsymbol{h}_{n,k}] = 0. \tag{77}$$

In the computations performed in this paper, the Gâteaux-derivative $D_\chi \mathcal{P}'(\chi_{n,k-1}, \tilde{\boldsymbol{u}})[\boldsymbol{h}_{n,k}]$ is approximated numerically. Then, the RMA is performed according to the scheme in Algorithm 1.

GPA: The functionality of the GPA is outlined in Algorithm 2, where the notation

$$\mathcal{P}_{n,k,l} = \mathcal{P}(\chi_{n,k}, \boldsymbol{B}_{\text{p}n,l}, \tilde{\boldsymbol{u}}), \qquad \mathcal{G}_{n,k,l} = \mathcal{G}(\chi_{n,k}, \boldsymbol{B}_{\text{p}n,l}), \tag{78a}$$

$$\mathbb{B}_{n,k,l} = \frac{\partial \hat{\boldsymbol{P}}}{\partial \boldsymbol{B}_{\text{p}}}(\chi_{n,k}, \boldsymbol{B}_{\text{p}n,l}), \qquad \mathbb{Y}_{n,k,l} = \frac{\partial \mathcal{G}}{\partial \boldsymbol{B}_{\text{p}}}(\chi_{n,k}, \boldsymbol{B}_{\text{p}n,l}), \tag{78b}$$

has been used. As explained in Section 6.1, the index l enumerates, at each time step, the iterations performed to linearise the equations with respect to $\boldsymbol{B}_{\mathrm{p}n}$. At the lth iteration, $\boldsymbol{B}_{\mathrm{p}n,l}$ is computed as shown in (57), and the increment $\boldsymbol{\Phi}_{n,l}$ is determined by (61). To control the linearisation error introduced by this procedure, line 15 of Algorithm 2 is mandatory. As for the RMA, the Gâteaux-derivative in line 22 of Algorithm 2 is approximated by computing the numerical derivative of the defect equation in line 8.

Algorithm 1 Solving the balance equation using the 'RMA'

1: **if** $X \in \partial\mathcal{B}_{\mathrm{D}}$ **then**
2: $\quad \boldsymbol{F}_{n,0} = T\chi_{\mathrm{b}n}$;
3: **else**
4: $\quad \boldsymbol{F}_{n,0} = \boldsymbol{F}(\chi_{n-1}(X))$;
5: **end if**
6: $k = 0$;
7:
8: $(\boldsymbol{P}_{n,k}, \boldsymbol{B}_{\mathrm{p}n}) = \mathrm{RMA}(\boldsymbol{F}_{n,k}, \boldsymbol{B}_{\mathrm{p}(n-1)})$;
9:
10: $r_{n,k} := -\mathcal{P}'_{n,k} = -\int_{\mathcal{B}} \boldsymbol{P}_{n,k} : \boldsymbol{g}\mathrm{Grad}\tilde{\boldsymbol{u}}$;
11:
12: **if** $\|r_{n,k}\| \leq \epsilon_F$ **then**
13: $\quad (\boldsymbol{F}_n, \boldsymbol{B}_{\mathrm{p}n}) = (\boldsymbol{F}_{n,k}, \boldsymbol{B}_{\mathrm{p}n})$;
14: **else**
15: $\quad$ determine $\boldsymbol{h}_{n,k+1}$ by solving:
16: $\quad D_\chi \mathcal{P}'_{n,k}[\boldsymbol{h}_{n,k+1}] = r_{n,k}$;
17:
18: $\quad \boldsymbol{F}_{n,k+1} = \boldsymbol{F}_{n,k} + D_\chi \boldsymbol{F}_{n,k}[\boldsymbol{h}_{n,k+1}]$;
19: $\quad k = k + 1$;
20: $\quad$ go to 8;
21: **end if**

Algorithm 2 Solving the balance equation using the 'GPA'

1: **if** $X \in \partial\mathcal{B}_{\mathrm{D}}$ **then**
2: $\quad \boldsymbol{F}_{n,0} = T\chi_{\mathrm{b}n}$;
3: **else**
4: $\quad \boldsymbol{F}_{n,0} = \boldsymbol{F}(\chi_{n-1}(X))$;
5: **end if**
6: $l = 0$; $\boldsymbol{B}_{\mathrm{p}n,0} = \boldsymbol{B}_{\mathrm{p}(n-1)}$;
7: $k = 0$;
8: $r_{n,k,l} := -\mathcal{P}_{n,k,l} + \int_{\mathcal{B}} \boldsymbol{g}\mathrm{Grad}\tilde{\boldsymbol{u}} : \mathbb{B}_{n,k,l}(\mathbb{Y}_{n,k,l})^{-1} : \mathcal{G}_{n,k,l}$;
9:
10: **if** $\|r_{n,k,l}\| \leq \epsilon_F$ **then**
11: $\quad$ compute $\boldsymbol{\Phi}_{n,l+1}$:
12: $\quad \boldsymbol{\Phi}_{n,l+1} = -(\mathbb{Y}_{n,k,l})^{-1} : \mathcal{G}_{n,k,l}$;
13: $\quad \boldsymbol{B}_{\mathrm{p}n,l+1} = \boldsymbol{B}_{\mathrm{p}n,l} + \boldsymbol{\Phi}_{n,l+1}$;
14:
15: $\quad$ **if** $\left\|\mathcal{G}(\boldsymbol{F}_{n,k}, \boldsymbol{B}_{\mathrm{p}_{n,l+1}})\right\| \leq \epsilon_{B_{\mathrm{p}}}$ **then**
16: $\quad\quad (\boldsymbol{F}_n, \boldsymbol{B}_{\mathrm{p}n}) = (\boldsymbol{F}_{n,k}, \boldsymbol{B}_{\mathrm{p}n,l+1})$;
17: $\quad$ **else**
18: $\quad\quad l = l + 1$; go to 8;
19: $\quad$ **end if**
20: **else**
21: $\quad$ determine $\boldsymbol{h}_{n,k+1}$ by solving:
22: $\quad D_\chi r_{n,k,l}[\boldsymbol{h}_{n,k+1}] = -r_{n,k,l}$.
23:
24: $\quad \boldsymbol{F}_{n,k+1} = \boldsymbol{F}_{n,k} + D_\chi \boldsymbol{F}_{n,k}[\boldsymbol{h}_{n,k+1}]$;
25: $\quad k = k + 1$; go to 8;
26: **end if**

7.1.2 Computational Effort

Even for the simple case of a unit cube, a good mesh resolution is required to obtain reliable results [56]. To this end, 32768 trilinear hexahedral elements have been used, which lead to 262144 non-linear problems in $\mathbb{R}^7$ (indeed, the unknowns of the problems are six independent components of $\boldsymbol{B}_{\mathrm{p}}$ and the Lagrange multiplier γ_τ, the latter being computed with an 8-point Gauß quadrature rule) at every integration point for the defect evaluation and the computation of the consistent tangent. 'Level 4' denotes the finest grid, which consists of 32768 hexahedral elements, and is found by a threefold, uniform refinement of the coarsest grid, 'Level 1', consisting of 64 hexahedral elements. The solving strategies adopted in this paper are similar to those reported in [56]. The non-linear variational problem in χ_n (which involves 107811 unknowns) is solved by applying the Newton method and having recourse to numerical differentiation to approximate the tangent operators. The linear sub-problems occurring within the Newton-iterations are solved by a preconditioned Bi-CGSTAB method, in which the preconditioner is determined by means of a multigrid cycle with a multigrid method. A Gauß-Seidel method served as smoother in the geometric multigrid cycle. The non-linear convergence is ensured by means of a line-search method.

It is important to remark that, for the GPA, additional effort has to be taken into

account to compute the increments $\boldsymbol{\Phi}_{n,l}$, which require the inversion of a fourth-order tensor at every integration point. Therefore, the generalised algorithm developed in this paper needs more computing time than the classical RMA (see Table 3). On the other hand, this increase of computational time can be viewed as a measure of the "weight" of the simplifying hypotheses (39) and (40) discussed in Section 5, right after equation (41).

Table 3: Computing time (in CPU-h) for using the RMA resp. the GPA in the shear-compression test.

	Level 1	Level 2	Level 3	Level 4
RMA	0.010	0.111	0.950	9.042
GPA	0.040	0.429	3.281	33.172

For the von Mises J_2 plasticity model presented in problem 'Pr1', only one iteration step in l, cf. Algorithm 2, was necessary to achieve a prescribed tolerance of $\epsilon_{\boldsymbol{B}_{\mathrm{p}}} = 1 \cdot 10^{-8}$ in the computations performed in this paper.

7.2 Comparison with the RMA for the Necking of a Circular Bar

The sample has initial length $L_0 = 26.667$ mm and initial radius $R_0 = 6.413$ mm. In cylindrical coordinates, $X = (R, \Theta, Z)$, $R \in [0, R_0]$, $\Theta \in [0, 2\pi)$, $Z \in [-L_0/2, L_0/2]$ denote, respectively, the radial coordinate, the angle about the symmetry axis, and the axial coordinate of the original geometry (initial configuration) of the specimen. The material parameters are listed in Table 1. A description of this very well-documented problem can be found, for example, in [15, 56, 66].

By exploiting the cylindrical symmetry of the bar, and assigning appropriate boundary conditions, the computations can be performed on one eight of the original geometry. However, the computational grid in the necking region is refined to a greater degree than in the rest of the specimen.

As suggested in [15], a non-linear hardening law is chosen. In particular, the hardening potential is taken to be

$$\hat{\mathfrak{H}}_\kappa(\alpha) = \tfrac{1}{2} H \alpha^2 + (H_\infty - \tau_y)\alpha + (H_\infty - \tau_y)\tfrac{1}{\omega}\left[\exp(-\omega\alpha) - 1\right], \tag{79a}$$

$$q = -K(\alpha) = -\frac{\partial \hat{\mathfrak{H}}_\kappa}{\partial \alpha}(\alpha) = -\left[H\alpha + (H_\infty - \tau_y)\left(1 - \exp(-\omega\alpha)\right)\right]. \tag{79b}$$

It should thus be necessary to apply a local Newton method to determine the plastic multiplier $\gamma_{\tau n}$ in (49) in every global Newton iteration for χ_n. However, in order to reduce the computational effort, and since $\gamma_{\tau n}$ can be viewed as a functional of χ_n through $\boldsymbol{F}_n$ (cf. (49)), $\gamma_{\tau n}$ is computed explicitly with respect to χ_n in every global Newton step.

The necking test is performed by applying to the specimen an axial displacement up to $\chi^z_{\mathrm{b}}(X, T) - Z = 7.0$ mm (which corresponds to an elongation of about 26% of the original length), for all $X \in [0, R_0] \times [0, 2\pi) \times \{L_0/2\} \cup [0, R_0] \times [0, 2\pi) \times \{-L_0/2\}$, which constitutes the Dirichlet-boundary. The final load is reached by several incremental loading steps.

7.2.1 Grid Refinement

The base-level, termed 'Level 1', consists of 120 hexahedral elements and the finer levels are generated by regular refinement of the grid. For instance, Level 2 is similar to the grid presented in [67].

To obtain results in good agreement with those reported in [15], a fine computational grid with 61440 hexahedral elements was needed for the computations performed in this

paper. Such a fine grid was necessary to approximate adequately the physical behaviour and the change of geometry of the specimen (cf. Figures 2(a) and 2(b)). One reason for the necessity of such a refinement lies in the fact that volumetric locking effects, which might arise as a consequence of the hypothesis of isochoric plastic flow, need to be avoided. Another common approach to eliminate volumetric locking is to increase the polynomial order of the finite element spaces [68, 69] instead of decreasing the mesh size. Figure 2(d) shows that a good accuracy of the experimental data can already be obtained on grid level 2 by using quadratic finite element *ansatz* functions.

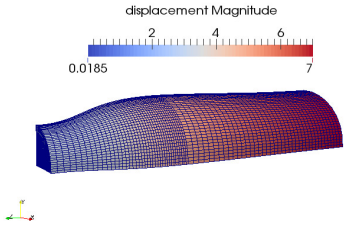

(a) Deformation of the circular bar ($\frac{1}{8}$ of the original geometry) in a tensile test with $\chi_{\mathrm{b}}^{z}(X,T) - Z = 7.0$ mm, $X \in [0,R_0] \times [0,2\pi) \times \{L_0/2\} \cup [0,R_0] \times [0,2\pi) \times \{-L_0/2\}$.

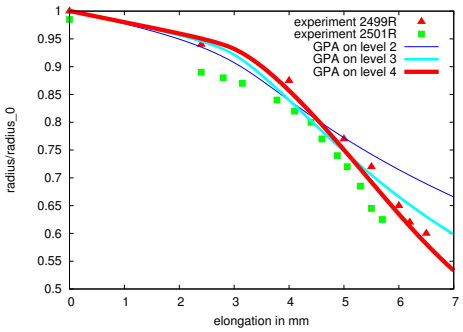

(b) Different refinement levels

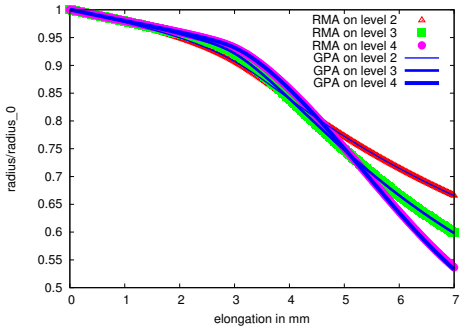

(c) Comparison of RMA and GPA

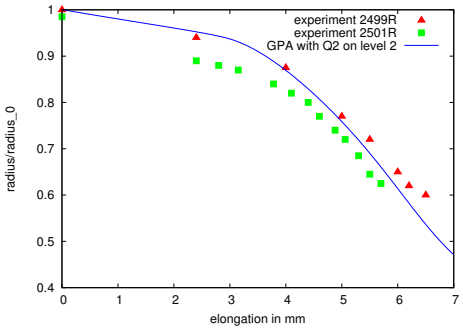

(d) Computation with quadratic finite element ansatz functions

Figure 2: Comparison of the numerical results obtained in this work for the necking test to the experimental data reported in [70]. The experiments 2499R (21 °C) and 2501R (71 °C) differ from each other in the temperature of the specimen. The change of the sectional area where necking occurs is plotted against the elongation in mm.

7.2.2 Convergence

In Table 4, pointwise changes in the components of the displacement and in the normal components of the Cauchy stress tensor $\boldsymbol{\sigma} = J^{-1}\boldsymbol{P}\boldsymbol{F}^{\mathrm{T}}$ are shown under uniform grid refinement. Although almost 200000 degrees of freedom are assigned on Level 4, the region in which plastic evolution takes place is still not captured correctly (cf. Table 4). Nevertheless, linear convergence behaviour for the displacements and the normal stresses can be observed at some representative sample points.

To discuss the convergence properties of the RMA and the GPA, it is necessary to look at the Algorithms 1 and 2, and to recall that, in both cases, a non-linear problem in the motion χ_n has to be solved at each time step. In particular, the RMA solves (53c), while the GPA solves $\Delta_{\mathcal{P}} = 0$, where $\Delta_{\mathcal{P}}$ is given in (62). Due to the high non-linearity of the

Table 4: Let $P_1 = (6.413, 0, 13.334)$; $P_2 = (6.413, 0, 10)$; $P_3 = (6.406, 0.785, 12)$ be three sample points of the specimen expressed in cylindrical coordinates; $w^r := \chi^r(P,t) - \chi^r(P,0)$ is the radial displacement and $w^z := \chi^z(P,t) - \chi^z(P,0)$ is the longitudinal displacement at $P \in \{P_1, P_2, P_3\}$ and $t = 280$ s.

	elements	DoFs	plastic IPs	$w^r(P_1,t)$	diff.	$w^r(P_2,t)$	diff.	$w^z(P_3,t)$	diff.
Level 1	120	627	960	-1.548		-0.794		-1.815	
					0.590		0.194		0.997
Level 2	960	3843	4709	-2.138		-0.600		-2.812	
					0.423		0.170		0.469
Level 3	7680	26691	25539	-2.561		-0.530		-3.281	
					0.412		0.009		0.100
Level 4	70080	198531	110908	-2.973		-0.541		-3.381	

	$\sigma^{rr}(P_1,t)$	diff.	$\sigma^r(P_2,t)$	diff.	$\sigma^{zz}(P_3,t)$	diff.
Level 1	3.646_{+03}		5.734_{+03}		3.860_{+03}	
		1.099_{+03}		2.297_{+03}		8.277_{+03}
Level 2	2.547_{+03}		8.031_{+03}		12.137_{+03}	
		0.489_{+03}		4.558_{+03}		3.475_{+03}
Level 3	2.058_{+03}		3.473_{+03}		8.662_{+03}	
		0.316_{+03}		0.687_{+03}		0.710_{+03}
Level 4	1.742_{+03}		2.786_{+03}		7.952_{+03}	

equations, iterative linearisation schemes are employed. These introduce *residuals* at each iteration. For the RMA, the residual introduced at the kth iteration is denoted by $r_{n,k}$ (see line 10 of the Algorithm 1). For the GPA, the residual at the iterations k and l is denoted by $r_{n,k,l}$ (see line 8 of the Algorithm 2). Both the iterative schemes used in this paper converge, since the norm of the residual is smaller than, or equal to, a prescribed tolerance (cf. line 12 of Algorithm 1 for the RMA, and line 10 of Algorithm 2 for the GPA). It is also important, however, to establish how fast the iterative methods converge. This can be done by counting the number of iteration steps required for satisfying the conditions $\|r_{n,k}\| \leq \epsilon_F$ (line 12 of Algorithm 1) and $\|r_{n,k,l}\| \leq \epsilon_F$ (line 10 of Algorithm 2). Looking at Table 5, it can be observed that the non-linear convergence rates of the RMA and the GPA are comparable. For both algorithms, a line-search method is evident in the first iteration steps for achieving convergence. Moreover, in both cases the convergence is quadratic.

Table 5: Comparison of the non-linear reduction of the norm (absolute value, in the present context) of the residual as computed by the RMA and the GPA for the necking test on Level 4. The residual is the right-hand-side of line 10 of the Algorithm 1 for the RMA, and of line 8 of the Algorithm 2 for the GPA. The load applied at the Dirichlet boundary of the cylinder is $\chi^z_{\mathrm{b}}(X,t) - Z = 7\frac{t}{T}$ mm, with $T = 280$ s.

RMA	$t = 1$ s	$t = 280$ s	**GPA**	$t = 1$ s	$t = 280$ s
nonlinear iteration step: 1	1.08_{+04}	1.05_{+04}	nonlinear iteration step: 1	1.07_{+04}	1.05_{+04}
2	6.81_{+02}	6.34_{+02}	2	1.07_{+03}	8.58_{+02}
3	5.51_{+02}	5.48_{+02}	3	3.20_{+02}	8.24_{+02}
4	5.50_{+00}	4.37_{+02}	4	7.72_{+01}	3.92_{+02}
5	5.26_{-02}	2.70_{+02}	5	7.63_{-01}	6.44_{+01}
6	4.63_{-04}	2.15_{+01}	6	5.42_{-03}	4.65_{+00}
7	2.86_{-06}	1.01_{+01}	7	3.91_{-05}	1.48_{-01}
8	2.54_{-08}	7.64_{-01}	8	3.53_{-07}	1.96_{-02}
9	3.53_{-10}	5.99_{-02}	9	2.39_{-09}	6.04_{-04}
10		3.04_{-03}	10		9.79_{-06}
11		4.11_{-05}	11		8.67_{-08}
12		1.40_{-06}	12		7.12_{-09}
13		1.55_{-08}			
14		6.58_{-09}			

7.3 Shear-compression Test for a biomechanical example

To outline the wider field of application of the GPA in comparison to the classical RMA, a biological flow rule of the form of (33) is chosen, i.e.

$$\dot{\boldsymbol{B}}_{\mathrm{p}} = -2\gamma_{\mathrm{p}} \boldsymbol{B}_{\mathrm{p}} \boldsymbol{G} \frac{\mathrm{dev}(\boldsymbol{\Sigma}_{\mathrm{R}})}{\|\mathrm{dev}(\boldsymbol{\tau})\|}, \tag{80a}$$

$$\gamma_{\mathrm{p}} := \lambda \left[\|\mathrm{dev}(\boldsymbol{\tau})\| - \sqrt{(2/3)}\tau_y \right]_+ . \tag{80b}$$

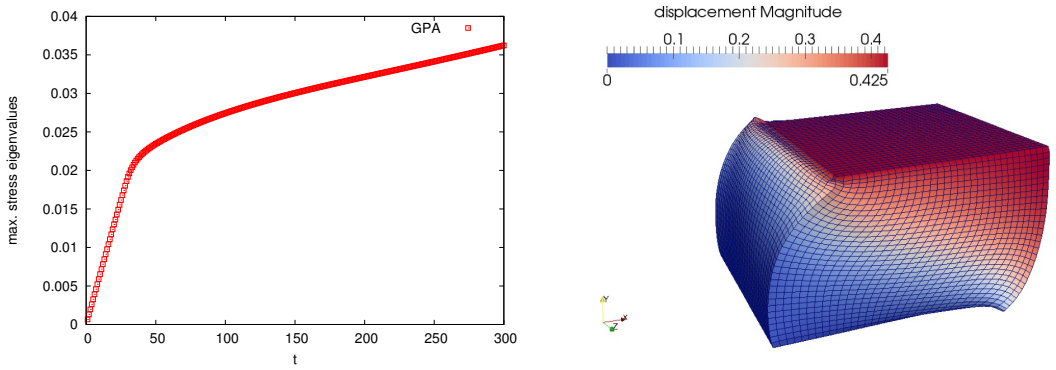

Figure 3: (Left) Maximal eigenvalue of $\boldsymbol{\tau}_\kappa$ at $X = (0.5, 0.5, 0.5)$ using the 'GPA' with $T = 300$ s. (Right) Deformation of the unit cube in a shear compression test for the biomechanical model at $t = T = 300$ s.

The mechanical response of the considered soft tissue, which is assumed to be hyperelastic, is modelled by means of the Holmes-Mow strain energy density function [71, 72, 73, 74]

$$\hat{W}_\kappa(\boldsymbol{C}_\mathrm{e}) = \alpha_0 \left([\hat{I}_3(\boldsymbol{C}_\mathrm{e})]^{-\beta} \exp\left\{ \alpha_1 [\hat{I}_1(\boldsymbol{C}_\mathrm{e}) - 3] + \alpha_2 [\hat{I}_2(\boldsymbol{C}_\mathrm{e}) - 3] \right\} - 1 \right) . \tag{81}$$

In (81), α_0 is a referential value of the strain energy density function, α_1, α_2 and β are model parameters, while $\hat{I}_1$, $\hat{I}_2$ and $\hat{I}_3$ are defined in (16a)–(16c). Clearly, $\hat{W}_\kappa$ describes a material exhibiting isotropic elastic properties with respect to the natural state. As done in problem 'Pr2', $\hat{W}_\kappa$ is a function of $\boldsymbol{C}_\mathrm{e}$ only. Moreover, hardening is disregarded here.

Since this model is based on the problem formulation 'Pr2', the application of the RMA in its classical form is not possible. Consequently, the GPA is validated for this biomechanical problem using the shear-compression test of the unit cube of section 7.1. The incremental load at the boundary is described by the Dirichlet boundary conditions (76). The material parameters used for this test are reported in Table 6. The elastic parameters α_0, α_1, and α_2 comply with the work of García and Cortés [72], who studied a model of articular cartilage. We selected β in such a way that $\beta = \alpha_1 + 2\alpha_2$ (cf. [71]). The material parameters incorporated in the phenomenological flow rule (80), which is suitable for biomechanical problems, are chosen in consistency with [58]. The computational grid consists of 32768 hexahedral elements.

Table 6: Material parameters

α_0 (N/mm^2)	α_1	α_2	β	λ	τ_y (N/mm^2)
0.722	0.150	0.024	0.198	0.500	0.020

The deformation of the cube in the shear-compression test is similar to that from Section 7.1 at time $t = T = 300$ s (cf. Figure 1 and Figure 3). However, the maximal eigenvalue of the Kirchhoff stress tensor $\boldsymbol{\tau}_\kappa$ at the midpoint of the unit cube differs from that found by the Neo-Hookean model (cf. Figure 1), and is plotted in Figure 3.

7.4 Software Framework UG4

The numerical methods presented in this work have been implemented in UG4, a novel version of the software framework UG ('Unstructured Grids') [75]. This toolbox provides fast, massive-parallel solvers for coupled partial differential equations like, e.g. geometric and algebraic multigrid methods. Its new tools for parallel communication (PCL) allow for an efficient scaling of the code on large numbers of processors [76].

8 Discussion and Outlook

As stated at the end of section 5.2, the algorithm proposed in this work treats $\boldsymbol{B}_{\mathrm{p}}$ and χ as equally ranked variables, even though technical reasons lead to a 'hierarchical' solution strategy, which suggests to compute first the plastic increment, $\boldsymbol{\Phi}_{n,l}$, by solving (60b), and then to determine the increment of deformation, $\boldsymbol{h}_{n,k}$, by solving the problem (68). These reasons are also related to the fact that the weak form of the momentum balance law is solved by a Finite Element method, whereas the flow rule is defined pointwise and, as such, requires no spatial discretisation (rather, $\boldsymbol{B}_{\mathrm{p}}$ is evaluated only at the integration points of the finite elements). The philosophy of the algorithm has been inspired by the observation that the modelling choices proposed in [16, 17] comply with the development of some generalised numerical procedures (cf., e.g., [77]) that tend to improve the efficiency of the 'standard' algorithms of Computational Plasticity. In the authors' opinion, this conceptual framework is suitable for a unified approach to the analysis of anelastic processes.

The theory reported in [16, 17] is based on the fundamental concept according to which a body that deforms and changes its internal structure is characterised by a "multi-layer kinematics" [17]. The kinematic descriptor associated with the "visible" motion of the body is the "standard velocity" $\boldsymbol{v}$ (or $\boldsymbol{u}$), while the kinematic descriptor accounting for the variation of the body's internal structure is the generalised velocity $\boldsymbol{L}_{\mathrm{p}} = \dot{\boldsymbol{F}}_{\mathrm{p}}\boldsymbol{F}_{\mathrm{p}}^{-1}$ (or $\dot{\boldsymbol{B}}_{\mathrm{p}}$). Consistently with the concept of "multi-layer kinematics", the space of generalised virtual velocities is generally a subset of

$$\tilde{\mathcal{H}}_{\mathrm{a}} := \{(\tilde{\boldsymbol{u}}, \tilde{\boldsymbol{L}}_{\mathrm{p}}) \in T\mathcal{S} \times (T\mathcal{C}_\kappa \otimes T^*\mathcal{C}_\kappa) \mid \tilde{\boldsymbol{u}}_{|\partial\mathcal{B}_{\mathrm{D}}} = \boldsymbol{0}\}\,, \tag{82}$$

where the subscript 'a' indicates that $\tilde{\mathcal{H}}_{\mathrm{a}}$ is obtained by augmenting $\tilde{\mathcal{H}}$ with $\tilde{\boldsymbol{L}}_{\mathrm{p}}$ (cf. (6)). It is important to remark that, in this framework, $\boldsymbol{F}_{\mathrm{p}}$ is not an internal variable. This strong difference with the standard theory requires to reformulate the Principle of Virtual Powers. Indeed, a logical consequence of viewing $\tilde{\boldsymbol{L}}_{\mathrm{p}}$ as a virtual velocity is that one has to introduce the external and internal forces, $\boldsymbol{M}_{\mathrm{ext}}$ and $\boldsymbol{M}_{\mathrm{int}}$, power-conjugate with $\tilde{\boldsymbol{L}}_{\mathrm{p}}$. Thus, if the material constitutive behaviour is of grade zero with respect to $\boldsymbol{F}_{\mathrm{p}}$ and of grade one in χ, one obtains

$$\mathcal{P}_{\mathrm{ext}}(\tilde{\boldsymbol{u}}, \tilde{\boldsymbol{L}}_{\mathrm{p}}) := \int_{\mathcal{B}} \boldsymbol{b}_{\mathrm{R}}.\tilde{\boldsymbol{u}} \;+\; \int_{\partial\mathcal{B}_{\mathrm{N}}} \boldsymbol{f}_{\mathrm{R}}.\tilde{\boldsymbol{u}} \;+\; \int_{\mathcal{B}} \boldsymbol{M}_{\mathrm{ext}} : \boldsymbol{\eta}\tilde{\boldsymbol{L}}_{\mathrm{p}}\,, \tag{83a}$$

$$\mathcal{P}_{\mathrm{int}}(\tilde{\boldsymbol{u}}, \tilde{\boldsymbol{L}}_{\mathrm{p}}) := \int_{\mathcal{B}} \boldsymbol{P} : \boldsymbol{g}\mathrm{Grad}\tilde{\boldsymbol{u}} \;+\; \int_{\mathcal{B}} \boldsymbol{M}_{\mathrm{int}} : \boldsymbol{\eta}\tilde{\boldsymbol{L}}_{\mathrm{p}}\,. \tag{83b}$$

By enforcing the PVP, i.e. setting $\tilde{\mathcal{P}}_{\mathrm{int}}(\tilde{\boldsymbol{u}}, \tilde{\boldsymbol{L}}_{\mathrm{p}}) = \tilde{\mathcal{P}}_{\mathrm{ext}}(\tilde{\boldsymbol{u}}, \tilde{\boldsymbol{L}}_{\mathrm{p}})$ for all $(\tilde{\boldsymbol{u}}, \tilde{\boldsymbol{L}}_{\mathrm{p}}) \in \tilde{\mathcal{H}}_{\mathrm{a}}$, the local force balance $\boldsymbol{M}_{\mathrm{int}} = \boldsymbol{M}_{\mathrm{ext}}$ is obtained, in conjunction with the standard one given in (9a)–(9c). Moreover, in the case of isochoric plastic distortions, and in the absence of hardening, the plastic dissipation reads $(\boldsymbol{M}_{\mathrm{int}} + \boldsymbol{\Sigma}) : \boldsymbol{\eta}\boldsymbol{L}_{\mathrm{p}} \geq 0$, which suggests to express $\boldsymbol{M}_{\mathrm{int}}$ as the sum of a dissipative stress $\boldsymbol{Y}$ and the negative of the Mandel stress tensor $\boldsymbol{\Sigma}$, so that $\boldsymbol{M}_{\mathrm{int}} = \boldsymbol{Y} - \boldsymbol{\Sigma}$. This result, together with the force balance $\boldsymbol{M}_{\mathrm{int}} = \boldsymbol{M}_{\mathrm{ext}}$, leads to $\boldsymbol{Y} = \boldsymbol{M}_{\mathrm{ext}} + \boldsymbol{\Sigma}$ [16, 17]. If, for simplicity, $\boldsymbol{M}_{\mathrm{ext}}$ is assumed to vanish, then the more stringent equality $\boldsymbol{Y} = \boldsymbol{\Sigma}$ is obtained. The latter equality is consistent with the standard theory, where the plastic dissipation is identified with $\boldsymbol{\Sigma} : \boldsymbol{\eta}\boldsymbol{L}_{\mathrm{p}}$.

In the case of vanishing external forces, the PVP can be rewritten as

$$\int_{\mathcal{B}} \boldsymbol{P} : \boldsymbol{g}\mathrm{Grad}\tilde{\boldsymbol{u}} \;+\; \int_{\mathcal{B}} (\boldsymbol{Y} - \boldsymbol{\Sigma}) : \boldsymbol{\eta}\tilde{\boldsymbol{L}}_{\mathrm{p}} = 0 \qquad \forall\, (\tilde{\boldsymbol{u}}, \tilde{\boldsymbol{L}}_{\mathrm{p}}) \in \tilde{\mathcal{H}}_{\mathrm{a}}\,. \tag{84}$$

When $\boldsymbol{Y}$ can be determined constitutively as a function $\boldsymbol{L}_{\mathrm{p}}$ [20, 36, 42, 43], the PVP (84) produces a system of coupled equations in the unknowns χ and $\boldsymbol{F}_{\mathrm{p}}$. Since the equation

determining $\boldsymbol{F}_{\mathrm{p}}$ stems from the second summand of (84), which is not local, suitable finite element basis functions for $\boldsymbol{F}_{\mathrm{p}}$ and $\tilde{\boldsymbol{L}}_{\mathrm{p}}$ should be introduced, as it is done for χ and $\tilde{\boldsymbol{u}}$. In particular, the algebraic form of the mixed problem (84), obtained after the finite element discretisation and linearisation of (84), leads to a block matrix, in which the extra-diagonal blocks couple the degress of freedom related to the standard deformation with those related to the plastic distortions. The same conclusions could be drawn also in the case of rate-independent plastic behaviour, by substituting the second term of (84) with the weak form of some flow rule [77]. As a consequence of this approach, $\boldsymbol{F}_{\mathrm{p}}$ need not be evaluated only at the integration points, as it happens in the standard theory.

If, on the one hand, the formulation (84) can be viewed as a reinterpretation of the standard theory of Elastoplasticity, on the other hand, spatial discretisations for $\boldsymbol{F}_{\mathrm{p}}$ become mandatory for those constitutive theories whose grade in $\boldsymbol{F}_{\mathrm{p}}$ is higher than the zeroth. This could happen, for instance, within the theory of defects in elasto-plastic materials (cf., e.g., [78]). In this case, indeed, the Differential Geometry tools required by the theory, like the Bilby-type connection $\left(\boldsymbol{A}^{(\mathrm{p})}\right)^{A}_{\ BD} = (\boldsymbol{F}_{\mathrm{p}}^{-1})^{A}_{\ \beta}\partial_{X^D}(\boldsymbol{F}_{\mathrm{p}})^{\beta}_{\ B}$, involve the differentiation of $\boldsymbol{F}_{\mathrm{p}}$ with respect to material coordinates. In such situations, or even in those in which the evolution law for $\boldsymbol{F}_{\mathrm{p}}$ is given by [79]

$$\dot{\boldsymbol{F}}_{\mathrm{p}} = \boldsymbol{Z}(\boldsymbol{F}_{\mathrm{p}}, \mathscr{R}_{\mathrm{p}}, \mathrm{Grad}\mathscr{R}_{\mathrm{p}}, X)\,, \tag{85}$$

where $\mathscr{R}_{\mathrm{p}}$ is the fourth-order curvature tensor associated with the plastic metric tensor $\boldsymbol{C}_{\mathrm{p}} = \boldsymbol{F}_{\mathrm{p}}^{\mathrm{T}}\boldsymbol{\eta}\boldsymbol{F}_{\mathrm{p}}$, spatial discretisations for $\boldsymbol{F}_{\mathrm{p}}$ and $\tilde{\boldsymbol{L}}_{\mathrm{p}}$ become necessary. In this respect, it might be useful to consider computational algorithms like the one proposed in this paper.

For the reasons outlined so far, the GPA seems to be a promising algorithm for those theories in which $\boldsymbol{F}_{\mathrm{p}}$ represents a structural degree of freedom, rather than an internal variable. As it currently stands, the GPA is actually a step forward in this direction. In a future work, the possibility of applying the GPA to such a two-field formulation of finite strain Plasticity shall be investigated in the framework of Poroplasticity, and together with the possibility of establishing robust solvers, whose efficiency has been already shown for optimisation problems and for the Navier-Stokes equations by means of a simultaneous solving process [80][81]. This could be an interesting approach for a further development of efficient solvers for structural mechanical problems.

Finally, the GPA could be a useful computational tool for problems in which plasticity is coupled with damage [82] as well as for biomechanical models of growth and tissue adaptation involving higher order gradients of the deformation (see, e.g., [83, 84, 85, 86]), for problems of remodelling of bone [87] and fibre-reinforced biological materials [88], and also for studying problems involving the mechanical interaction between fluid and porous matrix in compacting fluid-saturated grounds [89].

Acknowledgments

The Authors acknowledge the Goethe-Universität Frankfurt am Main (Germany), the German Ministry for Economy and Technology (BMWi), contract 02E10326 [AG and GW], the Baden-Württemberg-Stiftung [RP], and the Polytechnic of Turin, (Italy) [AG].

References

[1] Lubliner, J. *Plasticity Theory.* Dover Publications, Inc., Mineola, New York, 2008.

[2] Mićunović, MV. *Thermomechanics of viscoplasticity—fundamentals and applications.* Gao, DY, Ogden, RW. (Eds.), Advances in Mechanics and Mathematics. Heidelberg: Springer; 2009.

[3] Pinsky, PM, Ortiz, M, Pister, KS. Numerical integration of rate constitutive equations in finite deformation analysis. *Comput Methods Appl Mech Engng* 1983; 40: 137–158.

[4] Pinsky, PM, Ortiz, M, Taylor, RL. Operator split methods in the numerical solution of the finite deformation elastoplastic dynamic problem. *Comput Struct* 1983; 17(3): 345–359.

[5] Simo, JC, Ortiz, M. A unified approach to finite deformation elastoplasticity based on the use of hyperelastic constitutive equations. *Comput Methods Appl Mech Engng* 1985; 49: 221-245.

[6] Simo, JC. *Numerical Analysis and Simulation of Plasticity.* Handbook of Numerical Analysis, Vol. IV., Elsevier Science, 1998.

[7] Alberty, J, Carstensen, C, Zarrabi, D. Adaptive numerical analysis in primal elasto-plasticity with hardening. *Comput Methods Appl Mech Engng* 1999; 171: 175–204.

[8] Armero, F. Formulation of finite element implementation of multiplicative model of coupled poro-plasticity at finite strains under fully saturated conditions. *Comput Methods Appl Mech Engng* 1999; 171: 205–241.

[9] Han, W, Reddy, BD. *Plasticity – mathematical theory and numerical analysis.* Springer, New York, 1999.

[10] Toupin, RA. Elastic materials with couple stresses. *Arch Ration Mech Anal* 1962, 11: 385–414.

[11] Mindlin, RD. Micro-structure in linear elasticity. *Arch Ration Mech Anal* 1964, 16: 51–78.

[12] Mindlin, RD. Second gradient of strain and surface tension in linear elasticity. *Int J Solids Struct* 1965, 1: 417–438.

[13] Cleja-Tigoiu, S, Maugin, GA. Eshelby's stress tensors in finite elastoplasticity. *Acta Mech* 2000; 139: 231–249.

[14] Rice, JR. Inelastic constitutive relations for solids: an internal variable theory and its application to model plasticity. *J Mech Phys Solids* 1971; 19: 433–455.

[15] Simo, JC, Hughes, TJR. *Computational Inelasticity.* New York, Springer; 1998.

[16] Cermelli, P, Fried, E, Sellers, S. Configurational stress, yield and flow in rate-independent plasticity. *Proc R Soc A* 2001; A457: 1447–1467.

[17] DiCarlo, A, Quiligotti, S. Growth and balance. *Mech Res Commun* 2002; 29: 449–456.

[18] Mosler, J, Bruhns, OT. Towards variational constitutive updates for non-associative plasticity models at finite strain: models based on a volumetric-deviatoric split. *Int J Solids Struc* 2009; 46: 1676–1684.

[19] Rodriguez, EK, Hoger, A, McCullogh, AD. Stress-dependent finite growth in soft elastic tissues. *J Biomech* 1994; 27: 455–467.

[20] Epstein, M, Maugin, GA. Thermomechanics of volumetric growth in uniform bodies. *Int J Plasticity* 2000; 16: 951–978.

[21] Ambrosi, D, Mollica, F. On the mechanics of a growing tumor. *Int J Eng Sci*, 2002; 40: 1297–1316.

[22] Preziosi, L, Ambrosi, D, Verdier, C. An elasto-visco-plastic model of cell aggregates. *J Theor Biol*, 2010; 262(1): 35–47.

[23] Rajagopal, KR. Multiple configurations in continuum mechanics. *Rep Inst Comput Appl Mech* 1995; 6.

[24] Wieners, C. Nonlinear solution methods for infinitesimal perfect plasticity. *Z Angew Math Mech* 2007; 87:643–660.

[25] Marsden, JE, Hughes, TJR. *Mathematical Foundations of Elasticity.* New York: Dover Publications Inc.; 1983.

[26] Epstein, M. *The Geometric Language of Continuum Mechanics.* Cambridge: Cambridge University Press; 2010.

[27] Kröner, E. Allgemeine Kontinuumstheorie der Versetzungen und Eigenspannungen. *Arch Rational Mech Anal* 1959; 4: 273–334.

[28] Davini, C. Some remarks on the continuum theory of defects in solids. *Int J Solids Struct* 2001; 38: 1169–1182.

[29] Preston, S, Elżanowski, M. Material uniformity and the concept of the stress space. In: Bettina Albers (Ed.), *Continuous Media with Microstructure* (Collection in Honor of Krzysztof Wilmański), pp. 91–101. Heidelberg: Springer; 2010.

[30] Maugin, GA, Epstein, M. Geometrical material structure of elastoplasticity. *Int J Plasticity* 1998; 14: 90–115.

[31] Epstein, M, Elźanowski, M. *Material inhomogeneities and their evolution.* Berlin, Springer; 2007.

[32] Flory, PJ. Thermodynamic relations for high elastic materials. *Trans Faraday Soc* 1961; 41:8 29–838.

[33] Ogden, RW. Nearly isochoric deformations: Application to rubberlike solids. *J Mech Phys Solids* 1978; 26: 37–57.

[34] Lubarda, VA, Hoger, A. On the mechanics of solids with a growing mass. *Int J Sol Struct* 2002; 39: 4627–4664.

[35] Menzel, A. Modelling of anisotropic growth in biological tissues. A new approach and computational aspects. *Biomech Model Mechanobiol* 2005; 3: 147–171.

[36] Ambrosi, D, Guana, F. Stress-Modulated Growth. *Math Mech Solids* 2007; 12: 319–342.

[37] Liu, Y, Zhang, H, Zheng, Y, Zhang, S, Chen, B. A nonlinear finite element model for the stress analysis of soft solids with a growing mass. *Int J Sol Struc* 2014; 51(17): 2964–2978.

[38] Loret, B, Simões, FMF. A framework for deformation, generalized diffusion, mass transfer and growth in multi-spacies multi-phase biological tissues. *Eur J Mech A-Solid* 2005; 24: 757–781.

[39] Ambrosi, D, Guillou, A, Di Martino, ES. Stress-modulated remodeling of a non-homogeneous body. *Biomechan Model Mechanobiol* 2008; 7: 63–76.

[40] Grillo, A, Wittum, G, Giaquinta, G, Mićunović, MV. A multiscale analysis of growth and diffusion dynamics in biological materials. *Int J Eng Sci* 2009; 47: 261–283.

[41] Grillo, A, Federico, S, Wittum, G, Imatani, S, Giaquinta, G, Mićunović, MV. Evolution of a fibre-reinforced growing mixture. *Nuovo Cimento C* 2009; 32(1): 97–119.

[42] Ambrosi, D, Preziosi, L, Vitale, G. The insight of mixtures theory for growth and remodeling. *Z Angew Math Phys* 2010; 61: 177–191.

[43] Grillo, A, Federico, S, Wittum, G. Growth, mass transfer, and remodeling in fiber-reinforced, multi-constituent materials. *Int J Nonlinear Mech* 2012; 47: 388–401.

[44] Sciarra, G, dell'Isola, F, Hutter, K. A solid-fluid mixture model allowing for solid dilatation under external pressure. *Continuum Mechanics and Thermodynamics* 2001; 13(5): 287–306.

[45] Lubarda, VA. Constitutive theories based on the multiplicative decomposition of deformation gradient: Thermoelasticity, elastoplasticity, and biomechanics. *Appl Mech Rev* 2004; 57(2): 95–108.

[46] Simo, JC. A framework for finite strain elastoplasticity based on maximum plastic dissipation and the multiplicative decomposition: Part I. Continuum Formulation. *Comput Mech Appl M* 1988; 66:199–219.

[47] Bonet, J, Wood, RD. *Nonlinear Continuum Mechanics for Finite Element Analysis.* Cambridge, New York: Cambridge University Press; 2008.

[48] Epstein, M, Maugin, GA. The energy-momentum tensor and material uniformity in finite elasticity. *Acta Mech* 1990; 83: 127–133.

[49] Maugin, GA. *Material Inhomogeneities in Elasticity.* London: Chapman&Hall; 1993.

[50] Epstein, M, Maugin, GA. On the geometrical material structure of anelasticity. *Acta Mech* 1996; 115(1/4): 119–131.

[51] Cleja-Tigoiu, S. Yield criteria in anisotropic finite elasto-plasticity. *Arch. Mech* 2005; 57: 81–102.

[52] Cleja-Tigoiu, S, Iancu, L. Orientational Anisotropy and Plastic Spin in Finite Elasto-Plasticity. *Int J Sol Struc* 2011; 48(6): 939–952.

[53] Cleja-Tigoiu, S, Iancu, L. Orientational anisotropy and strength-differential effect in orthotropic elasto-plastic materials. *Int J Plasticity* 2013; 47: 80-110.

[54] Montáns, FJ, Bathe, K-J. Computational issues in large strain elasto-plasticity: an algorithm for mixed hardening and plastic spin. *Int J Numer Meth Engng* 2005; 63:159–196.

[55] Gabriel, G, Bathe, K-J. Some Computational Issues in Large Strain Elasto-Plastic Analysis. *Computers and Structures* 1995; 56(2/3):249–267.

[56] Neff, P, Wieners, C. Comparison of models for finite plasticity: A numerical study. *Comput Visual Sci* 2003; 6:23–25.

[57] Mičunovič, M. Thermodynamical and self-consistent approach to inelastic ferromagnetic polycrystals. *Arch Mech* 2006; 58(4-5): 393–430.

[58] Giverso, C, Preziosi, L. Modelling the compression and reorganization of cell aggregates. *Math Med Biol* 2012; 29: 181–204.

[59] Salsa, S. *Partial Differential Equations in Action: From Modelling to Theory.* Milan; Heidelberg; New York: Springer, 2008.

[60] Hofstetter, G, Taylor, RL. Non-Associative Drucker-Prager Plasticity at Finite Strains. *Communications in Applied Numerical Methods* 1990; 6: 583–589.

[61] Quintanilla, R, Saccomandi, G. The Importance of the Compatibility of Nonlinear Constitutive Theories with Their Linear Counterpart, *J Appl Mech* 2007; 74: 455–460.

[62] Federico, S. Volumetric-Distortional Decomposition of Deformation and Elasticity Tensor. *Math Mech Solids* 2010; 15: 672–690.

[63] Federico, S. Covariant Formulation of the Tensor Algebra of Non-Linear Elasticity. *Int J Nonlin Mech* 2012; 47: 273–284.

[64] Vergori, L, Destrade, M, McGarry, P, Ogden, RW. On anisotropic elasticity and questions concerning its finite element implementation. *Comput Mech* 2013, 52: 1185–1197.

[65] Federico, S, Grillo A, Imatani, S. The linear elasticity tensor of incompressible materials. *Math Mech Solids* 2015; 20(6): 643–662.

[66] Needleman, A. A numerical study of necking in circular cylindric bars. *J Mech Phys Solids* 1972; 20:111-127.

[67] Simo, JC, Armero, F. Geometrically nonlinear enhanced strain mixed methods and the method of incompatible modes. *Int J Numer Meth Engng* 1992; 33: 1413-1449.

[68] Düster, A, Rank, E. A p-version finite element approach for two- and three-dimensional problems of the J_2 flow theory with non-linear isotropic hardening. *Int J Numer Meth Engng* 2002; 53: 49–63.

[69] Heisserer, U, Hartmann, S, Düster, A, Yosibash, Z. On volumetric locking-free behaviour of p-version finite elements under finite deformations. *Commun Numer Meth Engng* 2008; 24:1019-1032.

[70] Norris, DM, Moran, B, Scudder, JK, Quinones, DF. A computer simulation of the tension test. *J Mech Phys Solids* 1978; 26:1–19.

[71] Holmes, MH, Mow, VC. The nonlinear characteristics of soft gels and hydrated connective tissues in ultrafiltration. *J Biomech* 1990; 23(11): 1145–1156.

[72] García, JJ, Cortés, DH. A nonlinear biphasic viscohyperelastic model for articular cartilage. *J Biomech* 2006; 39: 2991–2998.

[73] Federico, S, Grillo, A. Elasticity and permeability of porous fibre-reinforced materials under large deformations. *Mechanics of Materials* 2012; 44: 58–71.

[74] Tomic, A, Grillo, A, Federico, S. Poroelastic materials reinforced by statistically oriented fibres—numerical implementation and application to articular cartilage. *IMA Journal of Applied Mathematics* 2014; DOI:10.1093/imamat/hxu039.

[75] Vogel, A, Reiter, S, Rupp, M, Nägel, A, Wittum, G. UG4 - A Novel Flexible Software System for Simulating PDE Based Models on High Performance Computers. *Comput Visual Sci* 2013; DOI: 10.1007/s00791-014-0232-9

[76] Reiter, S, Vogel, A, Heppner, I, Rupp, M, Wittum, G. A Massively Parallel Geometric Multigrid Solver on Hierarchically Distributed Grids. *Comput Visual Sci* 2013; 16(4): 151–164.

[77] Eve, RA, Reddy, BD. The variational formulation and solution of problems of finite-strain elastoplasticity based on the use of a dissipation function. *Int J Numer Meth Engng* 1994; 37: 1673–1695.

[78] Cleja-Tigoiu, S. Elasto-plastic materials with lattice defects modeled by second order deformations with non-zero curvature. *Int J Fract* 2010; 166: 61–75.

[79] Epstein, M. Self-driven continuous dislocations and growth. In: *Mechanics of Material Forces*, Advances in Mechanics and Mathematics, Volume 11, Chapter 13, 129–148.

[80] Schulz, V, Wittum, G. Transforming smoothers for PDE constrained optimization problems. *Comput Visual Sci* 2008; 11: 207–219.

[81] Wittum, G. On the convergence of multigrid methods with transforming smoothers, theory with application to the Navier-Stokes equations. *Numer Math* 1989; 54: 543–563.

[82] Contrafatto, L, Cuomo, M. A new thermodynamically consistent continuum model for hardening plasticity coupled with damage. *Int J Sol Struct*, 2002; 37: 3935–3964.

[83] Lekszycki, T, dell'Isola, F. A mixture model with evolving mass densities for describing synthesis and resorption phenomena in bones reconstructed with bio-resorbable materials. *Z Angew Math Mech* 2012; 92(6): 426–444.

[84] Madeo, A, Lekszycki, T, dell'Isola, F. A continuum model for the biomechanical interactions between living tissue and bio-resorbable graft after bone reconstructive surgery. *CR Mecanique* 2011; 339: 625–640.

[85] Madeo, A, dell'Isola, F, Darve, F. A continuum model for deformable, second gradient porous media partially saturated with compressible fluids. *J Mech Phys Solids* 2013; 61(11): 2196–2211.

[86] dell'Isola, F, Seppecher, P, Madeo, A. How contact interactions may depend on the shape of Cauchy cuts in Nth gradient continua: approach "á la D'Alembert". *Zeitschrift für Angewandte Mathematik und Physik* 2012; 63(6): 1119–1141.

[87] Giorgio, I, Andreaus, U, Madeo, A. The influence of difference loads on the remodeling process of a bone and bioresorbable material mixture with voids. *Continuum Mech Thermodyn* 2014; DOI: 10.1007/s00161-014-0397-y

[88] Grillo, A., Wittum, G., Tomic, A., Federico, S. Remodelling in statistically oriented fibre-reinforced materials and biological tissues *Math Mech Solids* 2014; DOI: 10.1177/1081286513515265

[89] dell'Isola, F, Rosa, L, Woźniak, Cz. A micro-structured continuum modelling compacting fluid-saturated grounds: the effects of pore-size scale parameter. *Acta Mechanica* 1998; 127(1-4): 165–182.